Interleukin-17 Receptor A1 Gene Knockout Causes Weight Loss and Reduction of Intestinal Metabolism-Related Genes in The Japanese Medaka, *Oryzias Latipes*

Yo Okamura
University of Miyazaki
Hiroshi Miyanishi
University of Miyazaki
Masato Kinoshita
Kyoto University
Tomoya Kono
University of Miyazaki
Masahiro Sakai
University of Miyazaki
Jun-ichi Hikima (jhikima@cc.miyazaki-u.ac.jp)
University of Miyazaki

Research Article

Keywords: Genome editing, interleukin-17 receptor A, Japanese medaka, metabolism, transcriptome analysis, weight loss

Posted Date: December 7th, 2020

DOI: https://doi.org/10.21203/rs.3.rs-114142/v1

Abstract

In the intestine, the host must be able to control the gut microbiota and efficiently absorb transiently supplied metabolites, at the risk of enormous infection. In mammals, the inflammatory cytokine interleukin (IL)-17A/F is one of the key mediators in the intestinal immune system. However, many functions of IL-17 in vertebrate intestines remain unclarified. In this study, we established a gene-knockout (KO) model of IL-17 receptor A1 (RA1), an IL-17A/F receptor, in Japanese medaka (*Oryzias latipes*) using genome editing technique and the phenotypes were compared to wild type (WT) based on transcriptome analyses. Upon hatching, homozygous IL-17RA1-KO medaka mutants showed no significant morphological abnormality. However, after 4 months, significant weight decreases and reduced survival rates were observed in IL-17RA1-KO medaka. Comparing gene-expression patterns in WT and IL-17RA1-KO medaka revealed that various metabolism- and immune-related genes were significantly down-regulated in IL-17RA1-KO medaka intestine, particularly genes related to mevalonate metabolism (*mvda*, *acat2*, *hmgcs1*, and *hmgcra*) and genes related to IL-17 signaling (such as *il17c*, *il17a/f1,* and *rorc*) were found to be decreased. These findings show that IL-17RA regulated immune- and various metabolism-related genes in the intestine for maintaining the health of Japanese medaka.

Introduction

Mucosal tissues are sites with the highest risk of bacterial infection, due to direct contact with the external environment. However, the mucosa harbors many indigenous bacteria, and its microbiome composition is very important for maintaining health. Therefore, in mucosal tissues, a unique and complicated immune system, in which the host immune system and the microbiome mutually regulate each other, has been established.

In particular, the intestinal tract is a key player in the relationship between the microbiome composition and the health of mucosal tissues [1]. It involves both the adaptive immune system, mediated through M cells that uptake antigens, and an extremely developed innate immune system, including the production of mucin and antimicrobial peptides (AMPs) [2,3]. In mammals, interleukin (IL)-17 is a key mediator of the production of mucins and AMPs. Currently, six family members of the IL-17 family (IL-17A–F) have been identified in mammals, and among these, IL-17A and F are known as key inflammatory cytokines that modulate the microbiome [4]. IL-17A and F induce pro-inflammatory cytokines such as IL-1β, IL-6, and TNF-α; the chemokines CXCL1, CXCL8, and CCL20; and AMPs, including defensin and calprotectin [5,6]. T helper 17 (Th17) cells (a subset of $CD4^+$ T cells) produce IL-17 and have been reported to markedly accumulate in the mammalian intestinal tract, and it is known that both transforming growth factor β and IL-6 are essential for Th17 differentiation [7]. Other than Th17 cells, it was recently revealed that IL-17 is produced from various types of immune cells, including lymphocytes, γδ-T cells, natural killer T cells, innate lymphoid cells, neutrophils, mast cells, and macrophages [5]. In mice, the presence of the intestinal microbes segmented filamentous bacteria (SFB) is crucial for Th17 cell differentiation; the presentation of SFB antigen by intestinal dendritic cells triggers an increase in intestinal Th17 cells [8,9]. Thus, it is

becoming clear that the IL-17-mediated immune system is highly and mutually linked to the gut microbiome.

The IL-17 receptor (IL-17R) family comprises five members (IL-17RA–E). These receptors have conserved structural features, including extracellular fibronectin type III (Fn III)-like domains and an intracellular region with structures similar to those of fibroblast growth factor, IL-17R, and Toll-IL-1R family domains. Of these members, IL-17RA has the broadest binding pattern with each IL-17 ligand. To date, IL-17RA has been shown to bind IL-17A, C, E, and F [10]. Generally, IL-17RA forms a heterodimer with IL-17RC before acting as a receptor for IL-17A or IL-17F, and before mediating signal transduction. In the intestine, IL-17RA is expressed by various types of cells, including epithelial cells, fibroblasts, keratinocytes, synoviocytes, endothelial cells, T cells, B cells, and macrophages [4]. In mammals, IL-17RA-knockout (KO) mice showed reduced expression levels of the defensin and regenerating islet-derived protein 3 genes (which encode AMPs) in their intestinal tracts, resulting in further effects on the composition of the microbiome [11]. Thus, the importance of IL-17-mediated innate immunity via IL-17RA in the mammalian intestinal tract is gradually being revealed.

Intestinal structures differ between teleost fish and mammals. The intestines of teleosts do not contain key enterocytes for intestinal immune responses, such as Paneth cells, mature M cells, and Peyer's patches [12]. Additionally, it was recently shown that teleost intestines have a membrane that is framed with chitin nanofibers inside the mucosal layer [13]. Based on these differences, it is thought that the intestinal immune system of teleosts contributes to the maintenance of intestinal homeostasis through unique mechanisms, when compared to mammals.

The Japanese medaka (*Oryzias latipes*) is a small teleost fish with a short life cycle that is widely used as a model organism [14]. In our previous study, we created a KO medaka strain with mutations in the *il17a/f1*, which are equivalent to mammalian IL-17A/F, to clarify the role of medaka IL-17A/F signaling in the intestinal tract. Phenotypic analyses of the intestines of the IL-17A/F1-KO medaka revealed reduction in antibacterial molecules such as transferrin a (*tfa*) and lysozyme (*lyz*), and various digestive enzyme genes such as elastase (*ela*) and phospholipase A2 group IB (*pla2g1b*). Furthermore, the composition of the gut microbiome of IL-17A/F1-KO medaka was different than that of wild-type (WT) medaka, indicating that IL-17A/F signaling controls the gut microbiome through the induction of various genes, apart from immunity-related genes [15]. Data from other studies also showed that bacterial infection can induce the expression of teleosts IL-17 ligands in the intestine [16,17]. Furthermore, teleost recombinant teleost IL-17A/F induced immune genes such as *il1β*, *il6*, and *β-defensin* (*defb3*) *in vitro*, as has been observed in mammals [18–20]. Thus, reports on the functionality of IL-17 ligands in teleosts suggest that IL-17 signaling is very important for the immune responses, from teleosts to mammals. However, information related to the functionality of IL-17 receptors is quite limited, when compared with the available data for the ligands.

Here, we investigated the role and mechanism of *il17ra* by establishing an IL-17RA1-KO medaka strain. We characterized gene-expression levels and functions in IL-17RA1-KO medaka by RNA-sequencing (RNA-seq) analysis of the intestines of WT and IL-17RA1-KO medaka. The anterior and posterior intestines were separately analyzed, considering that distinct differences in IL-17 signaling-related immune responses were previously reported for teleosts [21].

Results

Establishment of the IL-17RA1-KO medaka strain

To KO the *il17ra1*, we deleted a genomic region spanning from exon 1 to 7 of the medaka *il17ra1* (Fig. 1A). Three of the four designed crRNAs (crRNA1-2, crRNA7-1, and crRNA7-2) showed the high mutation efficiencies (Fig. S1). A mixture of these three crRNAs was injected back into medaka embryos to edit the genome. In this manner, we established IL-17RA1-KO medaka with approximately 5.4 kb of genome sequence deleted from exon 1 to 7. The deduced amino acid sequence of mutated IL-17RA1 lacked most parts of the extracellular domain (IL-17 fn III domain) predicted using the domain search tool, SMART 7 (http://smart.embl-heidelberg.de); the IL-17 fn III domain is important for binding IL-17 ligands (Fig. 1B). After microinjection, we obtained six mutant lines (KO line A–D, J, and K; Fig. S2A) with the same open-reading frame (ORF), as the 5¢ deletion occurred upstream of *il17ra1* start codon. Specifically, the *il17ra1* deletion started in the middle of the crRNA1-2 region (upstream of the original *il17ra1* start codon), and exons 1 to 6 were completely lost in each case (Fig. S2B). At the amino acid level, the deletion corresponded to most of the extracellular IL-17 Fn III domain, with the downstream amino residues causing no codon frame shift (Fig. S2C). The ORF amplicon of WT *il17ra1* was not amplified from the cDNA samples of IL-17RA1-KO medaka, whereas the remaining common region (1,491 bp) was amplified, and its sequence was confirmed by sequencing (Fig. S3A). Furthermore, qPCR analysis using a primer set designed against the common region of WT and mutated *il17ra1* confirmed significantly lower expression in the posterior intestine of IL-17RA1-KO medaka (Fig. S3B).

Weight loss in IL-17RA1-KO medaka

The established IL-17RA1-KO medaka line was bred with heterozygous medaka, and genotyping by the HMA method was used to confirm each generation (Fig. S2D). It was impossible to maintain the IL-17RA1-KO medaka lines by mating homologous mutants. Homozygous individuals in all KO lines were lean, and the females did not lay eggs. Of the six IL-17RA1-KO lines, KO line C was chosen as the main line because its breeding and proliferation were more stable. Genotype comparisons were performed between WT and mutant (heterozygous and homozygous) populations immediately after hatching (at 0–1 day post-hatching [dph]) and at 110–120 dph. Furthermore, we performed a genotype comparison with our previously established IL-17A/F1-KO medaka line. No abnormalities were observed at 0–1 dph in IL-17RA1-KO medaka (Fig. 2A). However, at 110–120 dph, only the homologous mutants of IL-17RA1-KO presented significant decreases in body weight (Fig. 2B, C), which were also observed in all obtained homologous-mutant KO lines of IL-17RA, other than line C (*i.e.*, lines A and K; Fig. S4). Furthermore, the

proportion of surviving homologous mutants was significantly lower at 110–120 dph than at 0–1 dph (Fig. 2D).

Notably, we observed that the intestinal tract of IL-17RA1-KO medaka was significantly shorter, than that of the WT and IL-17A/F1-KO medaka (Fig. 3A, B). Histological observation of HE-stained sections revealed dramatically thinner muscle layers under the intestinal epithelium in IL-17RA-KO medaka than that in WT and IL-17A/F1-KO medaka (Fig. 3C).

Medaka anterior intestines expressed genes related to lipid-metabolism pathways, as observed in mammalian small intestines

We next performed RNA-seq analysis to investigate functional differences between the anterior and posterior intestines of medaka, and to assess the influences of IL-17RA1 KO on downstream gene-expression levels. cDNA libraries constructed with tissue sections from anterior and posterior medaka intestines are represented in Fig. 4A. After removing low-quality reads, adaptors, and reads with a high content of unknown bases, we obtained an average of 30,840,974 (anterior intestine/WT), 30,156,147 (posterior intestine/WT), 43,545,422 (anterior intestine/IL-17RA1-KO) and 38,596,287 (posterior intestine/IL-17RA1-KO) reads from the indicated transcriptome libraries. After annotation, 20,710 genes in the WT anterior intestine, 21,529 genes in the RA1-KO anterior intestine, 20,990 genes in the WT posterior intestine, and 21,734 genes in the RA1-KO posterior intestine were detected in each library (Fig. 4B). The overall gene-expression levels in the anterior and posterior intestines showed different patterns, which also differed from those of WT and IL-17RA1-KO medaka (Fig. 4C). In WT intestines, 139 genes showed higher expression levels in the anterior intestine than in the posterior intestine, and 174 genes showed significantly higher expression in the posterior intestine than in the anterior intestine. Tables S2 and S3 display the top 50 genes with large expression differences in the anterior and posterior intestines, respectively. Of the 139 genes up-regulated in the anterior intestine, 74 were also showed significantly higher expression in the anterior intestine of IL-17RA-KO medaka than in the posterior intestine of KO medaka. Similarly, of the 174 genes that were significantly up-regulated in WT posterior intestine, 98 genes were also expressed in IL-17RA-KO posterior intestine (Fig. S5A). GO analysis of the upregulated genes suggested that the anterior intestine produced various metabolites, such as lipids, organic acids, oxoacid, and carboxylic acid. In contrast, in the posterior intestine, genes related to proteolysis and cellular catabolic processes were significantly up-regulated (Fig. S5B). Furthermore, enrichment analysis of KEGG pathways showed that the anterior intestine exhibited an enhancement of the “fat digestion and absorption” pathway of the mammalian small intestine (Fig. 5A, B). Notably, marked up-regulation of the apolipoprotein A-I (*apoa1b*), group XIIB secretory phospholipase A2-like protein (*pla2g12b*), and monoacylglycerol O-acyltransferase 2 (*mogat2*) genes in both WT and IL-17RA-KO medaka was also confirmed by qPCR (Fig. 5C–E). In contrast, KEGG enrichment analysis showed that the posterior intestine exhibited enhanced expression of genes in the “lysosome” pathway (Fig. 6A, B). Of the genes with remarkably higher expression in the WT posterior intestine, up-regulation of cathepsin B (*ctsbb*), neuraminidase 1 (*neu1*), and mannosidase alpha class 2B member 1 (*man2b1*) was confirmed by qPCR (Fig. 6C–E).

IL-17RA1-KO medaka exhibited decreased IL-17 signalingand decreased expression of various metabolism- and immune-related genes

A comparison of IL-17RA1-KO and WT medaka intestines revealed 290 DEGs with significant changes ($P < 0.05$) in the anterior intestine (up-regulated genes: 167, down-regulated genes: 123). In the posterior intestine, 205 genes were identified as DEGs (up-regulated genes: 124, down-regulated genes: 81), as shown in Fig. 7A. Of these DEGs, genes down-regulated or up-regulated by 3-fold are shown in Tables S4–S7. We detected 24 DEGs commonly down-regulated in both the anterior and posterior intestines of IL-17RA1-KO, as well as 35 DEGs commonly up-regulated in both intestinal regions (Fig. 7B). We further visualized interactions between DEGs using the String App in Cytoscape. We examined potential relationships between IL-17RA and the DEGs by adding IL-17RA to the analysis and localized many metabolism-related genes; 47 genes clustered together with IL-17RA among the 123 down-regulated DEGs. Interestingly, IL-17C (an IL-17RA ligand) and the Th17 master transcription factor, nuclear receptor ROR-alpha (*rorc*), were included in this relationship. Furthermore, 10 genes including mevalonate pathway-related genes, mevalonate diphosphate decarboxylase (*mvda*), acetyl-CoA acetyltransferase 2 (*acat2*), 3-hydroxy-3-methylglutaryl-CoA synthase 1 (*hmgcs1*), and 3-hydroxy-3-methylglutaryl-coenzyme A (*hmgcr*) showed particularly strong interactions (Fig. 8). These 47 genes are presented in Table 1.

Of the DEGs with increased expression in the anterior intestine, 102 genes formed a cluster containing IL-17RA. In particular, a series of collagen genes showed strong interactions (Fig. S6). Furthermore, among the DEGs that were significantly decreased in the posterior intestine, some were possibly related to IL-17RA1, including IL-17A/F1, growth arrest and DNA damage inducible alpha (*gadd45a*), chymotrypsin-like elastase family member 2A (*ela2*), neuraminidase 1 (*neu1*), and signal transducer and activator of transcription 3 (*stat3*) (Fig. S7A). However, we did not find a gene cluster among the elevated DEGs that interacted with IL-17RA (Fig. S7B).

Furthermore, GO analyses were performed on the DEGs using the DAVID program. Among the down-regulated DEGs in the anterior intestine of IL-17RA1-KO medaka, terms related to various metabolic process including lipid metabolism, steroid metabolism, lipid biosynthesis, and oxidation reduction were annotated in the biological process (BP) category. Of the immune terms, defense response (BP category) and cytokine binding (molecular function category) were also identified among the top 12 terms with the most hits (Fig. 9A). In contrast, among the down-regulated DEGs in the posterior intestine of IL-17RA1-KO, the most hits were obtained for proteolysis; hits were also obtained for lipid metabolism-related and oxidation-reduction terms, similar to those obtained for terms of the anterior intestine (Fig. 9B). Development of the circulatory and cardiovascular systems (Fig. S8A) were emphasized among the up-regulated DEGs in the anterior intestine of IL-17RA1-KO medaka, whereas oxidation-reduction process and organic acid metabolic process were the top two BP terms in the posterior intestine (Fig. S8B).

Among the down-regulated DEGs in the anterior intestine of IL-17RA1-KO medaka, KEGG pathway analysis revealed that four genes (*mvda*, *acat2*, *hmgcs1,* and *hmgcr*) were part of the mammalian mevalonate metabolic pathway (Fig. 10A). Down-regulated levels of *mvda, acat2* and *hmgcr* were

confirmed by qPCR analysis (Fig. 10B). The levels of IL-17 signaling-related genes were also confirmed by qPCR. RNA-seq analysis showed that the anterior intestine of IL-17RA1-KO, the master transcriptional factor of IL-17-producing lymphocytes (*rorc*) and *il17c* (an IL-17RA ligand). In posterior intestine of IL-17RA1-KO, *il17a/f1* (an IL-17RA ligand) was significantly down-regulated. Conversely, *stat3* shown to be down-regulated by RNA-seq analysis in the posterior intestine of IL-17RA-KO, did not show significant changes by qPCR analysis (Fig. 10C).

Comparison of RNA-seq results between IL-17A/F1-KO and IL-17RA1-KO medaka

Previously, we used IL-17A/F1, one of the ligands of IL-17RA knockout medaka (IL-17A/F1-KO) to reveal the role of IL-17 A/F signaling in the intestine and performed RNA-seq analysis of the whole intestinal tissues (GenBank accession number: DRA008715) [15]. Comparing the down-regulated DEGs between IL-17A/F1-KO and IL-17RA1-KO medaka intestines showed that protein disulfide isomerase family A, member 2 (*pdia2*) and cytochrome P450 family 51 subfamily A, polypeptide 1 (*cyp51*) were significantly down-regulated in IL-17A/F1-KO and in both sections of IL-17RA1-KO medaka intestines. Furthermore, the anterior and posterior intestines of IL-17RA1-KO shared eight and seven down-regulated genes with IL-17A/F1-KO medaka, respectively (Table 2).

Discussion

This study is the first to establish a mutant medaka line of the IL-17RA1 gene using the CRISPR–Cas9 genome-editing system, with comprehensive transcriptomic analyses. In our previous report, we revealed that medaka have two IL-17RA genes (IL-17RA1 and IL-17RA2) encoded on different chromosomes [22]. Synteny analysis suggested that the medaka IL-17RA1 is equivalent to the homologous mammalian IL-17RA gene, and qPCR analysis confirmed remarkably higher expression of IL-17RA1 than of IL-17RA2 in both the anterior and posterior intestines [22]. Thus, we selected IL-17RA1 as the target gene for further exploration in teleosts. In this study, IL-17RA1-KO medaka unexpectedly showed distinct phenotypes, unlike the IL-17A/F1-KO medaka examined in our previous study. These differences might reflect the broad functionality of the IL-17RA receptor. Of the IL-17 ligand family, IL-17A, C, E, and F are known to bind IL-17RA. The binding of each ligand to IL-17RA is determined by another IL-17 receptor that can form a complex with IL-17RA (*i.e.*, heterodimers of IL-17RA with IL-17RC, IL-17RB, and IL-17RE function as receptors for IL-17A/F, IL-17E, and IL-17C, respectively). IL-17C appeared to have an inflammation-inducing property (similar to IL-17A) and can induce inflammatory cytokines and AMPs such as IL-1β and defensin. However, unlike IL-17A/F, IL-17C is mainly produced by epithelial cells, rather than lymphocytes [23]. IL-17C expression has been reported in multiple teleost species, as has its ability to induce inflammatory cytokines such as IL-1β (similar to the mammalian counterpart), and up-regulated IL-17C expression has been reported during infection [24,25].

In contrast, IL-17E (IL-25) can be produced from not only Th17 cells, but also epithelial cells, mast cells, and Th2 cells. Furthermore, IL-17E shares the lowest homology with other IL-17 families and has been implicated in the IgA, IgE, and IgG1 production, and the cytokine responses of Th2 cells [26]. However, IL-

17E has not been found in teleosts. In addition, there have been limited reports on the functionality of IL-17C and IL-17E. Although IL-17RA and IL-17RD heterodimer formation has been clarified, the binding properties of these heterodimers and any associated ligand have not yet been reported. However, the intracellular site of the heterodimer can bind TRAF6, which is important for intracellular signal transduction [10,27]. Previous evidence suggests the presence of novel ligands that can signal through IL-17R. The findings of this study revealed a very interesting aspect of IL-17 ligands in immune responses, demonstrating that IL-17C and IL-17A/F1 were significantly down-regulated in IL-17RA1-KO medaka intestines.

During our transcriptomic analysis, we separately examined the anterior and posterior sections of medaka intestinal tissues. The digestive system of teleosts, including medaka, is structurally different from that of mammals. Teleosts contain no organ corresponding to the mammalian stomach with low-pH gastric juice, and there is no distinct separation of the small and large intestine in the intestinal tract [28]. Our results showed that in the anterior section of the medaka intestine, the number of genes specifically expressed in the mammalian small intestine was markedly higher than that of posterior section. Previous data showed that apolipoprotein, fatty acid binding protein 2, and monoacylglycerol acyltransferase were localized in the mammalian small intestine [29–31]. In the mammalian small intestine, digestive enzymes and absorbing epithelial cells mainly perform the metabolism and absorption of dietary nutrients [32]. However, in the posterior intestine of medaka, lysosome-related genes were expressed at dramatically higher levels, when compared with their corresponding levels in the anterior section. Previous histological data showed that intestinal epithelial cells containing a large number of vacuoles are locally concentrated in the posterior intestine of multiple teleost species [33,34].

Thus, the anterior intestine of medaka plays important roles in metabolism and nutrient absorption, similar to the small intestine of mammals. In the IL-17RA1-KO medaka, we made two noteworthy observations: the lost body weight of homologous mutant IL-17RA1-KO medaka and the significant down-regulation of various lipid metabolism-related genes in the anterior intestine. Indeed, multiple reports have demonstrated that IL-17 attenuation was accompanied by body weight loss in mice. In exposure tests using mice treated with dextran sulfate sodium, a model of inflammation model [35] or infected with *Chlamydia muridarum* [36], IL-17A attenuation using a neutralizing antibody caused more severe weight loss, when compared with control animals. Furthermore, the weight increase observed after feeding with a high-fat diet (HFD) was slower in IL-17A-KO mice than in WT mice [37], suggesting that IL-17A may be involved in lipid absorption. In addition, in teleosts, lipids are consumed as a primary energy source and excess triglycerides are stored in the liver, muscles, and adipose tissues [38]. In medaka, feeding with an HFD caused an increase in body weight, as seen in mammals [39]. Thus, the disruption of lipid metabolism in the anterior intestine may be one of the causes of weight loss in IL-17RA1-KO medaka.

In particular, of the metabolism-related genes with decreased expression in the anterior intestine of IL-17RA1-KO, the expression levels of several enzyme-encoding genes associated with mevalonate metabolism were reduced. Some human patients with mevalonate kinase (mvk) deficiency showed a

significant loss of body weight [40]. In addition, the loss of adipocytes via apoptosis was reported in mice with deficient mevalonate metabolism due to the adipocyte-specific KO of 3-hydroxy-3-methylglutaryl-CoA (HMG-CoA) reductase (HMGCR) [41]. These data indicate that mevalonate metabolism is very important for the establishment of lipid tissues. Moreover, isopentenyl diphosphate (IPP) synthesized downstream of the mevalonate-metabolism pathway is very important for the activation of γδ T cells, which are known as one of main IL-17-producing lymphocytes, and IPP is directly recognized by T-cell receptors [42]. The present results indicate a causal relationship with the decreased expression of several IL-17 pathway-related genes in IL-17RA-KO medaka. Future metabolome analyses are necessary to further clarify the relationship between IL-17 signaling and lipid metabolism in greater detail. Moreover, it is difficult to completely understand the causes of the weight loss observed in IL-17RA1-KO medaka by only analyzing the intestinal tissue. It is also important to focus on the liver and adipose tissue (which are important for metabolism) and the brain (which controls the appetite).

In conclusion, we established an IL-17RA1-KO medaka line and present the first report of an IL-17R-KO medaka line. IL-17RA1-KO medaka showed significant weight loss and decreased survival at 4 months after hatching. Furthermore, RNA-seq analyses revealed the down-regulation of various metabolic related genes, including a series of mevalonate pathway-related genes and IL-17 signaling-related genes, in the anterior intestine of IL-17RA1-KO medaka. Our result suggest that IL-17 signaling not only participates in immune responses, but also maintains intestinal homeostasis, such as lipid metabolism. However, in this study, we did not elucidate the genes encoding IL-17 ligand that bind to IL-17RA, which specifically modulate phenotypes, such as the observed weight decrease. Future studies are needed to establish KO strains of medaka for IL-17RA ligands other than IL-17A/F1 and to analyze in detail the effects of IL-17RA-mediated signal transduction on fish growth and health.

Material And Methods

Medaka

The Cab strain (Kyoto-Cab strain) of Japanese medaka was maintained in several transparent plastic tanks with a circulating water system (26°C) under a 14-h light and 10-h dark cycle. For gene-expression analysis, we used 4-month old WT and mutants (KO) fish, and weighing 100-200 mg. All animal experiments were conducted according to the relevant national (Act on Welfare and Management of Animals, Ministry of the Environment, Japan) and international guidelines. Ethics approval from the local Institutional Animal Care and Use Committee was not sought as this law does not mandate the protection of fish.

Body weight measurements and histological staining

Villus tissues of the intestinal tract were sampled from the anterior section of the intestine in 4-month-old adult fish. Intestinal tissues were fixed in 4% paraformaldehyde /0.1 M phosphate buffer solution and embedded in paraffin. Sections (8 μm) were stained with hematoxylin and eosin (HE) for microscopic

observations (20× magnification). WT and KO adult medaka (4 months old, n = 10) were anesthetized using MS 222 (Sigma-Aldrich, St. Louis, MO), and the water on their bodies was wiped off before weighing the medaka on a Sartorius Analytical Balance BP121S (Sartorius, Germany).

Establishment of IL-17RA1-KO medaka strains

Approximately 0.5 nL of a solution containing Synthetic CRISPR (cr) RNAs (25 ng/μL), trans-activating crRNA (40 ng/μL), and clustered regularly interspaced short palindromic repeats (CRISPR)- associated protein 9 (Cas9) mRNA (100 ng/μL) was injected into one- to two-cell stage embryos with a manipulator (Narishige, Tokyo, Japan). Two different crRNAs were designed to target exons 1 and 7 of the medaka IL-17RA1 gene and to delete approximately 5.4 kilobases (kb) (Fig. 1A). The sequences of four crRNAs are shown in Table S1. Genomic DNA (gDNA) was extracted from randomly selected embryos to confirm gene-editing efficiencies, using the heteroduplex mobility assay (HMA). Filial generation (F) 0 fish, grown from the injected fertilized eggs, were interbred with WT medaka (Cab strain) to produce F1 heterozygotes. Among the F1 fish, males and females carrying an identical mutation were mated (in-crossed) to obtain homozygous progeny and/or a mutant line (F2). HMA was performed to detect the mutated locus in the genome, and the mutant efficiency was confirmed. The sequences of polymerase chain reaction (PCR) primers used to generate products for the HMAs are shown in Table S1. Before collecting the gDNA samples, the medaka were anesthetized using MS-222 (Sigma-Aldrich). Briefly, gDNA was prepared from embryos or scraped body surfaces by dissolving the samples in 20 μL of a solution containing 0.2 mM EDTA and 25 mM NaOH, followed by incubation at 95°C for 20 min. The samples were neutralized with the same volume of 40 mM Tris/HCl (pH 8.0). Each gDNA-containing solution was used as a template for PCR, which was performed in 10-μL reactions containing 5 μL KOD One® PCR Master Mix (Toyobo, Osaka, Japan), 1 μL of gDNA-containing solution, 0.25 μL each of two forward primers (IL-17RAF1 and IL-17RAF2), and 0.5 μL of a reverse primer (IL-17RAR1). The primers were used at final concentrations of 5 pM. The PCR program was initially run at 94°C for 1 min, followed by 38 cycles of 94°C for 10 s, 66°C for 5 s, and 68°C for 5 s. The amplicons were separated by 12% polyacrylamide gel electrophoresis to compare their migration patterns.

2.4. RNA extraction and complementary DNA (cDNA) synthesis for next-generation sequencing and real-time quantitative PCR (qPCR) analysis

For qPCR analysis, total RNA was extracted from the whole intestines of adult medaka using an RNAiso Plus Kit (TaKaRa Bio, Kusatsu, Japan), according to manufacturer's instructions. For RNA-seq analysis, each intestinal section (anterior and posterior intestines) was dissected from three medaka and pooled together in the same tube (normalized). For each group, two sets of sample tubes containing three medaka intestine specimens each were subjected to RNA extraction, and equal volumes of total RNA (300 ng) from the two samples from the same group were mixed. The RNA concentrations were quantified with a NanoDrop spectrophotometer (Thermo Fisher Scientific, Waltham, MA, USA), and an optical-density ratio (260:280 nm) of 1.8 was set as the minimum quality cut-off value for RNA purity. The samples were sequenced using a Hi-Seq instrument by DNAFORM (Japan).

For qPCR analysis, RNA samples were extracted from individual medaka (n=3), and the concentration and quality of each sample were determined as described above. cDNA was synthesized using 200 ng of total RNA extracted from each sample using the ReverTra Ace qPCR RT Master Mix with gDNA Remover (Toyobo, Japan), according to manufacturer's instructions.

Sequence read mapping, differential-expression analysis, and gene-enrichment analysis

Processed reads were deposited in the DDBJ Sequence Read Archive under accession number DRA010584. Subsequently, the collected reads were mapped to the annotated medaka Hd-rR reference genome (release 85; http://www. ensembl.org/index.html) using the STAR program and further analyzed using the Feature Counts function. Transcriptional-expression values were estimated as fragments per kilobase of exon length per million reads, and transcripts with a *p*-value < 0.05 were considered to be significantly differentially expressed. After identifying genes exhibiting significant expression changes for each comparison, gene-enrichment analysis was performed using the Database for Annotation, Visualization and Integrated Discovery (DAVID) program [43]. Gene Ontology (GO) terms in the biological processes (GOTERM_BP_FAT), cellular component (GOTERM_CC_FAT), and molecular function (GOTERM_MF_FAT) categories, as well as Kyoto Encyclopedia of Genes and Genomes (KEGG) pathways, were selected.

Data visualization

Differences in the gene-expression levels ($\log_2$ fold-changes) related to each pathway map in the KEGG database was performed using the pathview package of R-studio software [44]. A heat map of all gene-expression levels was constructed using the software program, TCC-GUI. Gene interactions and networks were analyzed using String App database of Cytoscape (version 3.8.0) [45]. The String App database was used to predict interactions with each differently expressed gene (DEG), based on the presence of gene fusions, neighboring genes, co-occurrence, experimental findings, text mining, database analysis, and evidence of co-expression.

Gene-expression analysis by PCR and quantitative real-time PCR (qPCR)

qPCR was performed to analyze differences in expression patterns between WT and KO intestinal tissues. Total RNA was extracted from the intestines of medaka (n = 3 from each group), and their respective cDNAs were prepared separately as described in Section 2.3. Target genes for expression analysis were selected based on the RNA-seq results, and the sequences of the primers used are shown in Table S1. PCR amplification was performed to quantify the expression levels of genes located in the anterior or posterior intestines in 15-μL reactions containing 7.5 μL KOD One® PCR Master Mix, 1.5 μL cDNA (equally normalized cDNA from three medaka), 1.5 μL (5 pmol) each of the forward and reverse primers, and 3 μL distilled water. The PCR program was initially run at 94°C for 1 min, followed by 25 cycles of 94°C for 10 s, 63°C for 5 s, and 68°C for 5 s. qPCR amplification was conducted in triplicate in a total volume of 15 μL containing 7.5 μL Brilliant III Ultra-Fast SYBR® Green QPCR Master Mix (Agilent Technologies, Santa

Clara, CA), 1.5 µL cDNA (not normalized), and 1.5 µL (5 pmol) each of the forward and reverse primers. The qPCR program was run at 95°C for 15 s and 60°C for 30 s, followed by 40 cycles on a CFX connect TM (Bio-Rad Laboratories, Hercules, CA). Melting-curve analysis of the amplified products was performed after thermocycling was complete to confirm the specificity of amplification. The medaka *β-actin* (*actb*) gene served as an internal control to confirm the quality and quantity of cDNA. Relative expression ratios were calculated based on the comparative-cycle threshold (Ct) method ($2^{-\Delta\Delta CT}$ method). Using this method, the Ct values of target genes and the internal control were determined for each sample, after which the average Ct value from triplicate experiments was used to calculate expression levels, relative to that of *actb*. In statistical analysis, F-test were performed for checking the homogeneity of variance. For F-test, command of R-studio, var test (for two groups comparison) and Hartley test (for four groups comparison) were used respectively. Student *t*-test was used when homoscedasticity could be assumed between the two groups, and Welch t-test was used when it could not be assumed.

Abbreviations

AMP, antimicrobial peptide; Cas9, CRISPR-associated protein 9; CRISPR, clustered regularly interspaced short palindromic repeats; DAVID, Database for Annotation, Visualization and Integrated Discovery; DEG, differentially expressed gene; dph, day post-hatching; fn III, fibronectin type III; gDNA, genomic DNA; GO, Gene Ontology; HE, hematoxylin and eosin; HFD, high-fat diet; HMA, heteroduplex mobility assay; IL, interleukin; IL-17RA1, interleukin-17 receptor A1; kb, kilobase; KO, knockout; ORF, open-reading frame; PCR, polymerase chain reaction; qPCR, quantitative PCR; RNA-seq, RNA sequencing; SFB, segmented filamentous bacteria; Th, T helper; WT, wild-type

Declarations

Declarations of interest

None

Funding

This work was supported by a Grant-in-Aid for Scientific Research (A) and (B) from the Japan Society for the Promotion of Science (JSPS), Japan [grant numbers 17H01486 and 17H03863]. This work was also supported by a Grant-in-Aid for JSPS Research Fellows from JSPS, Japan [grant number 19J14996].

Author contributions

Conceptualization, YO, TK, MS, JH; Software, YO; Methodology, YO, HM, MK, JH; Visualization, YO, HM, TK, JH; Investigation, YO, HM; Resources, YO, MK; Data curation, YO, TK, JH; Validation, YO, TK, JH; Formal analysis, YO, HM, MK, JH; Project administration, YO, MS, JH; Supervision, MS, JH; Writing – original draft, YO, HM, MK, JH; Writing – review & editing, HM, MK, TK, MS, JH; Funding acquisition, MS, JH.

Acknowledgements

We would like to thank Editage (www.editage.jp) for English language editing.

References

1. Marchesi, J. R. *et al.* The gut microbiota and host health: A new clinical frontier. *Gut* **65**, 330–339 (2016).
2. Kau, A. L., Ahern, P. P., Griffin, N. W., Goodman, A. L. & Gordon, J. I. Human nutrition, the gut microbiome and the immune system. *Nature* **474**, 327–336 (2011).
3. Honda, K. & Littman, D. R. The microbiota in adaptive immune homeostasis and disease. *Nature* **535**, 75–84 (2016).
4. Iwakura, Y., Ishigame, H., Saijo, S. & Nakae, S. Functional specialization of interleukin-17 family members. *Immunity* **34**, 149–162 (2011).
5. Isailovic, N., Daigo, K., Mantovani, A. & Selmi, C. Interleukin-17 and innate immunity in infections and chronic inflammation. *J. Autoimmun.* **60**, 1–11 (2015).
6. Kirkham, B. W., Kavanaugh, A. & Reich, K. Interleukin-17A: A unique pathway in immune-mediated diseases: Psoriasis, psoriatic arthritis and rheumatoid arthritis. *Immunology* **141**, 133–142 (2014).
7. Ivanov, I. I. *et al.* The orphan nuclear receptor RORγt directs the differentiation program of proinflammatory IL-17 + T helper cells. *Cell* **126**, 1121–1133 (2006).
8. Ivanov, I. I. *et al.* Induction of intestinal Th17 cells by segmented filamentous bacteria. *Cell* **139**, 485–498 (2009).
9. Goto, Y. *et al.* Segmented filamentous bacteria antigens presented by intestinal dendritic cells drive mucosal Th17 cell differentiation. *Immunity* **40**, 594–607 (2014).
10. Li, J., Casanova, J. L. & Puel, A. Mucocutaneous IL-17 immunity in mice and humans: Host defense vs. excessive inflammation. *Mucosal Immunol.* **11**, 581–589 (2018).
11. Kumar, P. *et al.* Intestinal interleukin-17 receptor signaling mediates reciprocal control of the gut microbiota and autoimmune inflammation. *Immunity* **44**, 659–671 (2016).
12. Brugman, S. The zebrafish as a model to study intestinal inflammation. *Dev. Comp. Immunol.* **64**, *82*–92 (2016).
13. Nakashima, K. *et al.* Chitin-based barrier immunity and its loss predated mucus-colonization by indigenous gut microbiota. *Nat. Commun.* **9**, 3402 (2018).
14. Wittbrodt, J., Shima, A. & Schartl, M. Medaka - A model organism from the Far East. *Nat. Rev. Genet.* **3**, *53*–64 (2002).
15. Okamura, Y. *et al.* Interleukin-17A/F1 deficiency reduces antimicrobial gene expression and contributes to microbiome alterations in intestines of Japanese medaka (*Oryzias latipes*). *Front. Immunol.* **11**, 1–17 (2020).

16. Li, H. *et al.* Cloning and characterization of two duplicated interleukin-17A/F2 genes in common carp (*Cyprinus carpio L.*): Transcripts expression and bioactivity of recombinant IL-17A/F2. *Fish Shellfish Immunol.* **51**, *303*–312 (2016).
17. Mao, X. *et al.* Effects of *Vibrio harveyi* infection on serum biochemical parameters and expression profiles of interleukin-17 (IL-17) / interleukin-17 receptor (IL-17R) genes in spotted sea bass. *Dev. Comp. Immunol.* **110**, 103731 (2020).
18. Monte, M. M., Wang, T., Holland, J. W., Zou, J. & Secombes, C. J. Cloning and characterization of rainbow trout interleukin-17A/F2 (IL-17A/F2) and IL-17 receptor a: Expression during infection and bioactivity of recombinant IL-17A/F2. *Infect. Immun.* **81**, 340–353 (2013).
19. Du, L. *et al.* Identification and functional characterization of grass carp IL-17A/F1: An evaluation of the immunoregulatory role of teleost IL-17A/F1. *Dev. Comp. Immunol.* **51**, 202–211 (2015).
20. Takahashi, Y. *et al.* Interleukin-17A/F1 from Japanese pufferfish (*Takifugu rubripes*) stimulates the immune response in head kidney and intestinal cells. *Fish Shellfish Immunol.* **103**, 143–149 (2020).
21. Oehlers, S. H. *et al.* Topographical distribution of antimicrobial genes in the zebrafish intestine. *Dev. Comp. Immunol.* **35**, 385–391 (2011).
22. Okamura, Y. *et al.* Molecular characterization and expression of two interleukin-17 receptor A genes on different chromosomes in Japanese medaka, *Oryzias latipes*. *Comp. Biochem. Physiol. Part - B Biochem. Mol. Biol.* **240**, 110386 (2020).
23. Ramirez-Carrozzi, V. *et al.* IL-17C regulates the innate immune function of epithelial cells in an autocrine manner. *Nat. Immunol.* **12**, 1159–1166 (2011).
24. González-Fernández, C., Chaves-Pozo, E. & Cuesta, A. Identification and regulation of interleukin-17 (IL-17) family ligands in the teleost fish European sea bass. *Int. J. Mol. Sci.* **21**, 2439 (2020).
25. Ding, Y., Ao, J. & Chen, X. Comparative study of interleukin-17C (IL-17C) and IL-17D in large yellow croaker *Larimichthys crocea* reveals their similar but differential functional activity. *Dev. Comp. Immunol.* **76**, 34–44 (2017).
26. Pappu, R., Ramirez-Carrozzi, V. & Sambandam, A. The interleukin-17 cytokine family: Critical players in host defence and inflammatory diseases. *Immunology* **134**, *8*–16 (2011).
27. Rong, Z. *et al.* L-17RD (Sef or IL-17RLM) interacts with IL-17 receptor and mediates IL-17 signaling. *Cell Res.* **19**, 208–215 (2009).
28. Brugman, S. The zebrafish as a model to study intestinal inflammation. *Dev. Comp. Immunol.* **64**, 82–92 (2016).
29. Tokuhara, D. *et al.* Specific expression of apolipoprotein A-IV in the follicle-associated epithelium of the small intestine. *Dig. Dis. Sci.* **59**, 2682–2689 (2014).
30. Lockwood, J. F., Cao, J., Burn, P. & Shi, Y. Human intestinal monoacylglycerol acyltransferase: Differential features in tissue expression and activity. *Am. J. Physiol. - Endocrinol. Metab.* **285**, E927–E937 (2003).

31. Han, T. K. & So, W. Y. Effects of FABP2 ALA54Thr gene polymorphism on obesity and metabolic syndrome in middle-aged Korean women with abdominal obesity. *Cent. Eur. J. Public Health* **27**, 37–43 (2019).
32. Kiela, P. R. & Ghishan, F. K. Physiology of intestinal absorption and secretion. *Best Pract. Res. Clin. Gastroenterol.* **30**, 145–159 (2016).
33. Park, J. *et al.* Lysosome-rich enterocytes mediate protein absorption in the vertebrate gut. *Dev. Cell* **51**, *7*–20 (2019).
34. Iida, H. & Yamamoto, T. Morphological studies of the goldfish hindgut mucosa in organ culture. *Cell Tissue Res.* **238**, 523–528 (1984).
35. Song, X. *et al.* Growth Factor FGF2 Cooperates with interleukin-17 to repair intestinal epithelial damage. *Immunity* **43**, *488*–501 (2015).
36. Bai, H. *et al.* IL-17/Th17 Promotes Type 1 T cell immunity against pulmonary intracellular bacterial infection through modulating dendritic cell function. *J. Immunol.* **183**, 5886–5895 (2009).
37. Bi, Y. *et al.* IL-17A-dependent gut microbiota is essential for regulating diet-induced disorders in mice. *Sci. Bull.* **62**, 1052–1063 (2017).
38. Oishi, K. *et al.* Regulation of triglyceride metabolism in medaka (*Oryzias latipes*) hepatocytes by Neu3a sialidase. *Fish Physiol. Biochem.* **46**, 563–574 (2020).
39. Fujisawa, K. *et al.* Evaluation of the effects of L-carnitine on medaka (*Oryzias latipes*) fatty liver. *Sci. Rep.* **7**, 2749 (2017).
40. ter Haar, N. M. *et al.* The phenotype and genotype of mevalonate kinase deficiency: A series of 114 cases from the eurofever registry. *Arthritis Rheumatol.* **68**, 2795–2805 (2016).
41. Yeh, Y. S. *et al.* The mevalonate pathway is indispensable for adipocyte survival. *iScience* **9**, 175–191 (2018).
42. Xiang, Z. & Tu, W. Dual face of Vγ9Vdδ2-T cells in tumor immunology: Anti- versus pro-tumoral activities. *Front. Immunol.* **8**, 1041 (2017).
43. Huang, D. W., Sherman, B. T. & Lempicki, R. A. Systematic and integrative analysis of large gene lists using DAVID bioinformatics resources. *Nat. Protoc.* **4**, *44*–57 (2009).
44. R Core Team. R: A language and environment for statistical computing. *R Foundation for Statistical Computing*, Vienna (2018).
45. Shannon, P. *et al.* Cytoscape: A software Environment for integrated models of biomolecular interaction networks. *Genome Res.* **13**, 2498–2504 (2003).

Tables

Due to technical limitations, table 1,2 is only available as a download in the Supplemental Files section.

Figures

Fig. 1.

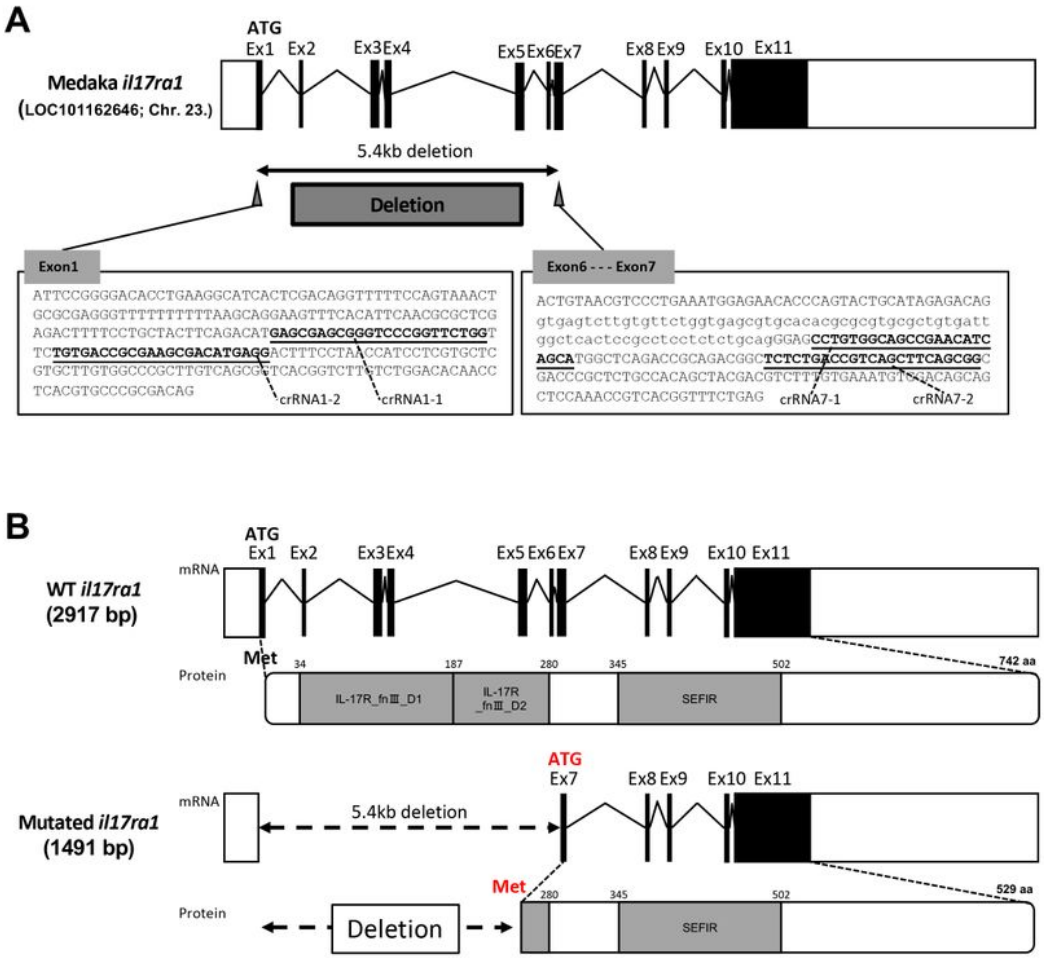

Figure 1

crRNA regions and comparison of the wild-type (WT) medaka interleukin-17 receptor A1 (il17ra1) gene with a mutated il17ra1. (A) Four crRNA regions in the medaka IL-17RA1 gene. Four crRNAs were designed against exons 1–7 of the il17ra1 (5.4-kilobase deletion). (B) Comparison of mutated il17ra1 with the WT il17ra1. Based on the deduced amino acid sequence, the mutated il17ra1 lacked most of the IL-1 fibronectin type (fn III) domain, which is the extracellular domain responsible for ligand binding. The

domain regions were predicted using the domain-prediction tool, SMART7. The residues of the extracellular and entire intracellular regions were the same as those of WT medaka il17ra1.

Fig. 1.

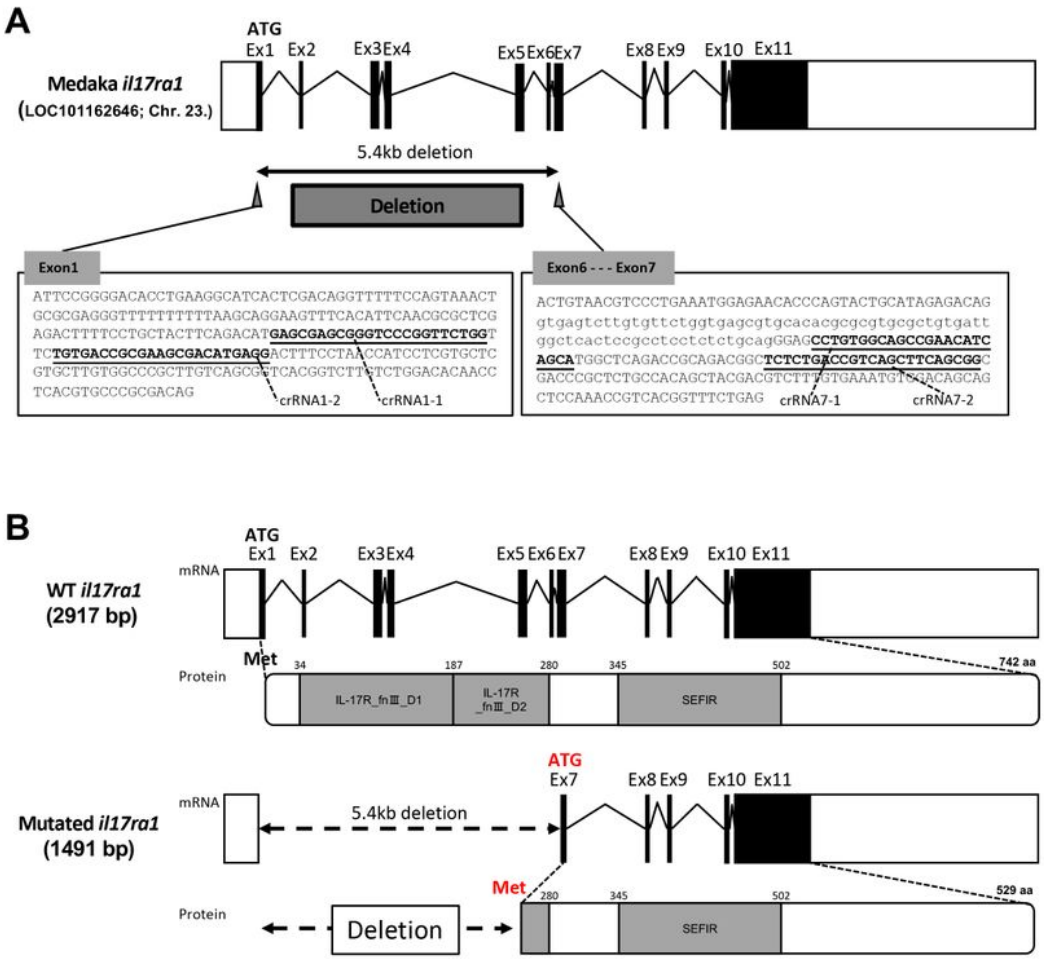

Figure 1

crRNA regions and comparison of the wild-type (WT) medaka interleukin-17 receptor A1 (il17ra1) gene with a mutated il17ra1. (A) Four crRNA regions in the medaka IL-17RA1 gene. Four crRNAs were designed against exons 1–7 of the il17ra1 (5.4-kilobase deletion). (B) Comparison of mutated il17ra1 with the WT

il17ra1. Based on the deduced amino acid sequence, the mutated il17ra1 lacked most of the IL-1 fibronectin type (fn III) domain, which is the extracellular domain responsible for ligand binding. The domain regions were predicted using the domain-prediction tool, SMART7. The residues of the extracellular and entire intracellular regions were the same as those of WT medaka il17ra1.

Fig. 2.

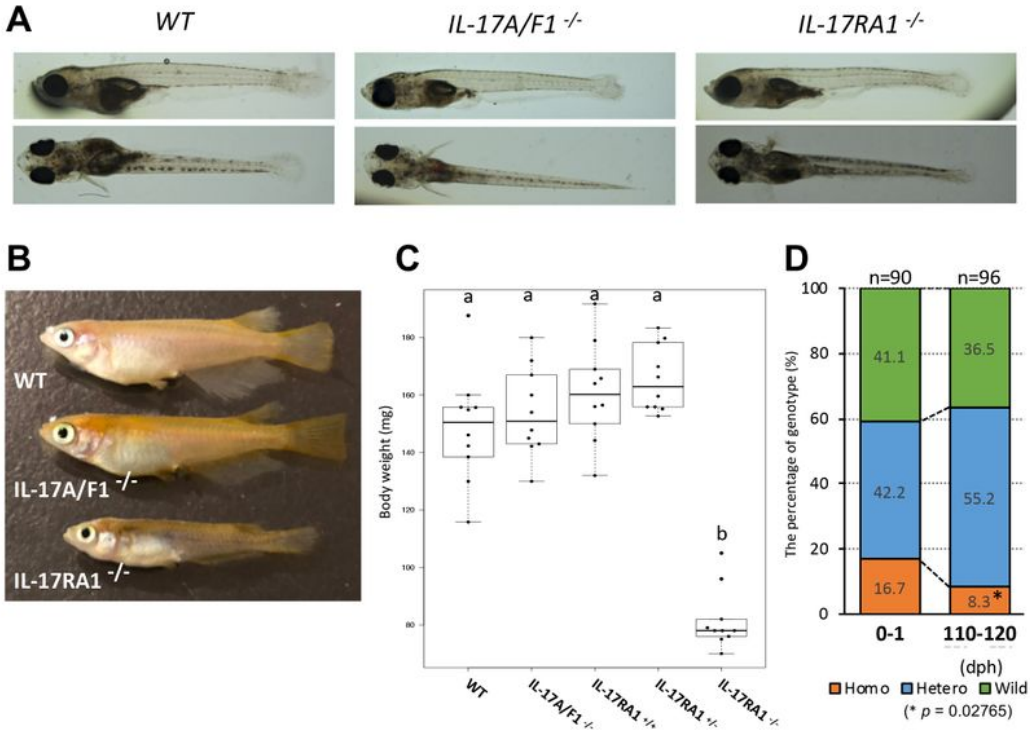

Figure 2

IL-17RA1-knockout (KO) medaka showed significant weight loss compared with WT and IL-17A/F1-KO medaka. (A–C) Comparison of medaka larvae at 0–1 day post-hatching (dph). No apparent differences were observed among WT, IL-17A/F1-KO, and IL-17RA1-KO medaka larvae at 0–1 dph (A), but severe weight loss was seen at 110–120 dph in IL-17RA1-KO medaka (B). Body weights were significantly lower only in homologous IL-17RA1-KO medaka, compared to those of WT medaka, medaka with homologous IL-17A/F1 mutants, and medaka with other genotypes. Different letters abovethe bars indicate significant difference at $P < 0.05$ as indicated by Tukey-Kramer multiple comparison tests after one-way ANOVA. The data shown were obtained in one experiment with three individual fish ($n = 5$). (D) The proportion of homologous IL-17RA1-KO medaka decreased significantly at 110–120 dph. The exact binomial test was used for statistical analysis in R-studio.

Fig. 2.

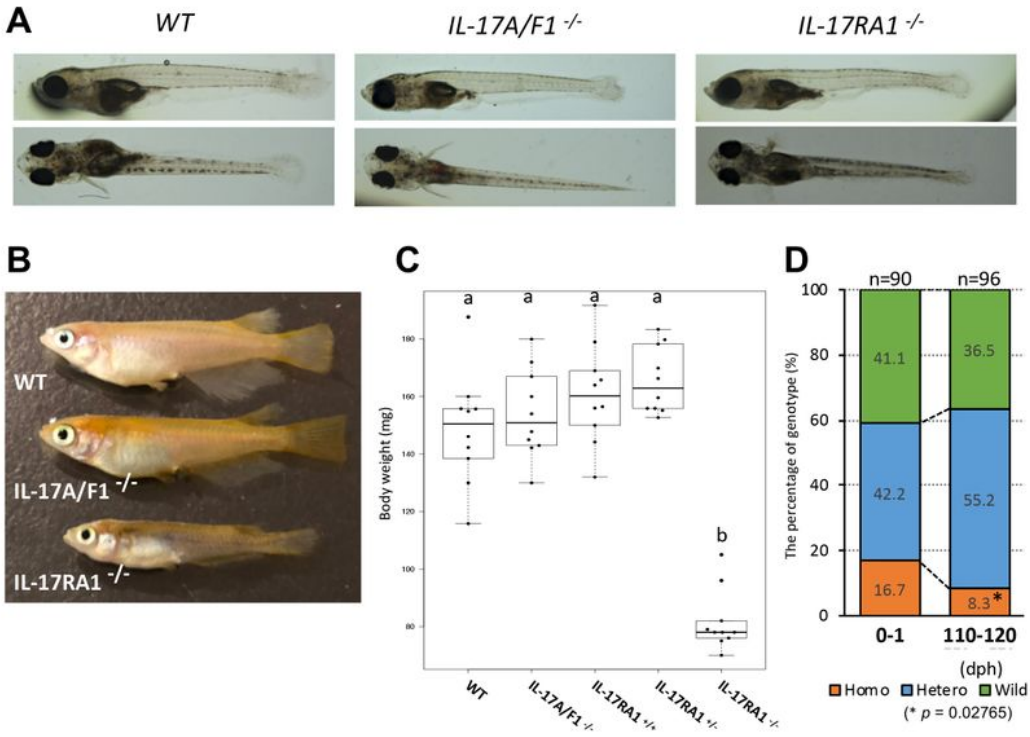

Figure 2

IL-17RA1-knockout (KO) medaka showed significant weight loss compared with WT and IL-17A/F1-KO medaka. (A–C) Comparison of medaka larvae at 0–1 day post-hatching (dph). No apparent differences were observed among WT, IL-17A/F1-KO, and IL-17RA1-KO medaka larvae at 0–1 dph (A), but severe weight loss was seen at 110–120 dph in IL-17RA1-KO medaka (B). Body weights were significantly lower only in homologous IL-17RA1-KO medaka, compared to those of WT medaka, medaka with homologous

IL-17A/F1 mutants, and medaka with other genotypes. Different letters abovethe bars indicate significant difference at $P < 0.05$ as indicated by Tukey-Kramer multiple comparison tests after one-way ANOVA. The data shown were obtained in one experiment with three individual fish (n = 5). (D) The proportion of homologous IL-17RA1-KO medaka decreased significantly at 110–120 dph. The exact binomial test was used for statistical analysis in R-studio.

Fig. 3.

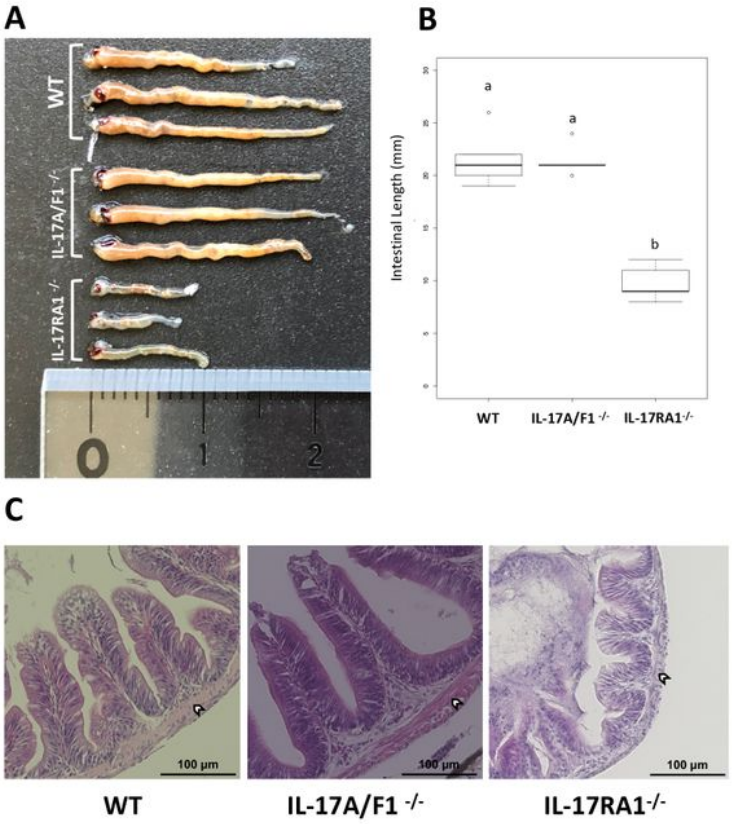

Figure 3

Comparisons of apparent differences in the intestinal tracts of WT, IL-17A/F1-KO, and IL-17RA1-KO medaka. (A, B) Comparison of the intestinal tract length. The intestinal tract of IL-17RA1-KO medaka was significantly shorter than that of WT and IL-17A/F1-KO medaka. (C) Hematoxylin and eosin staining of the anterior intestine. Histological changes in intestinal villus tissue were not observed in the intestinal tract of IL-17A/F1-KO medaka. However, thinner muscle layers under the intestinal villus were observed in IL-17RA1-KO medaka. The observed villus tissues of the intestinal tract were sampled from the anterior intestinal section of a 4-month-old adult fish. Different letters abovethe bars indicate significant difference at $P < 0.05$ as indicated by Tukey-Kramer multiple comparison tests after one-way ANOVA. The data shown were obtained in one experiment with three individual fish ($n = 5$).

Fig. 3.

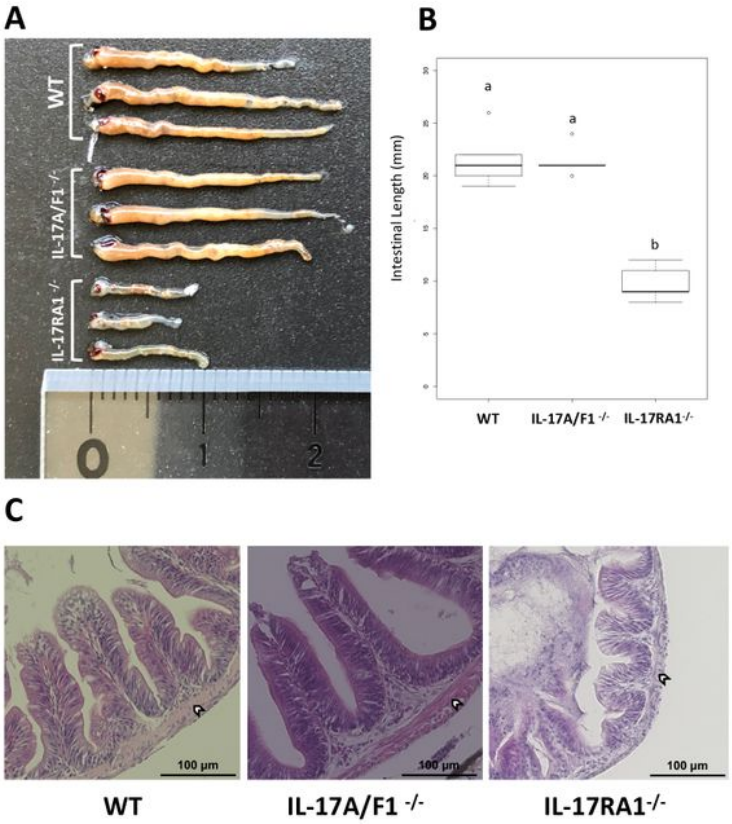

Figure 3

Comparisons of apparent differences in the intestinal tracts of WT, IL-17A/F1-KO, and IL-17RA1-KO medaka. (A, B) Comparison of the intestinal tract length. The intestinal tract of IL-17RA1-KO medaka was significantly shorter than that of WT and IL-17A/F1-KO medaka. (C) Hematoxylin and eosin staining of the anterior intestine. Histological changes in intestinal villus tissue were not observed in the intestinal tract of IL-17A/F1-KO medaka. However, thinner muscle layers under the intestinal villus were observed in

IL-17RA1-KO medaka. The observed villus tissues of the intestinal tract were sampled from the anterior intestinal section of a 4-month-old adult fish. Different letters abovethe bars indicate significant difference at P < 0.05 as indicated by Tukey-Kramer multiple comparison tests after one-way ANOVA. The data shown were obtained in one experiment with three individual fish (n = 5).

Fig. 4.

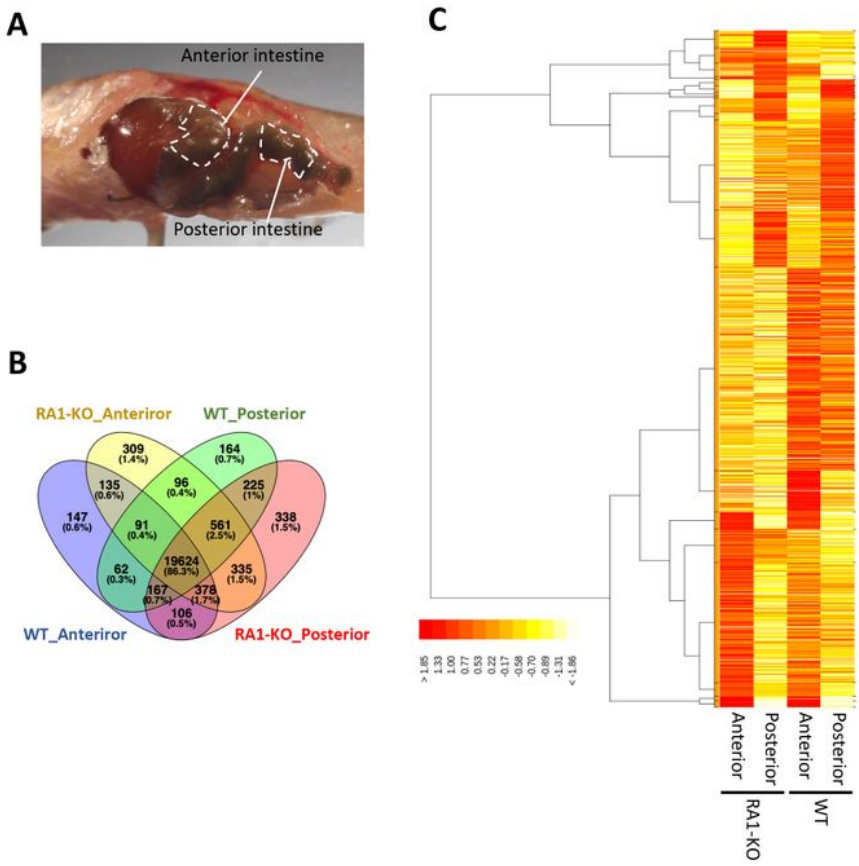

Figure 4

RNA-sequencing (RNA-seq) analysis of samples of the anterior and posterior intestines of WT and IL-17RA1-KO medaka. (A) Complementary DNA libraries were constructed with the selected intestines, as shown in the picture, and the analyzed samples were divided into two sections (anterior and posterior). (B–C) The overall gene-expression patterns are shown for each group (WT_Anterior, RA1-KO_Anterior, WT_Posterior, and RA1-KO Posterior). (B) The Venn diagram shows the numbers of expressed and overlapping genes expressed in each group. (C) A heat map was also used to visualize differences in the overall gene-expression patterns among the different groups. The heat map was constructed using TCC-GUI software.

Fig. 4.

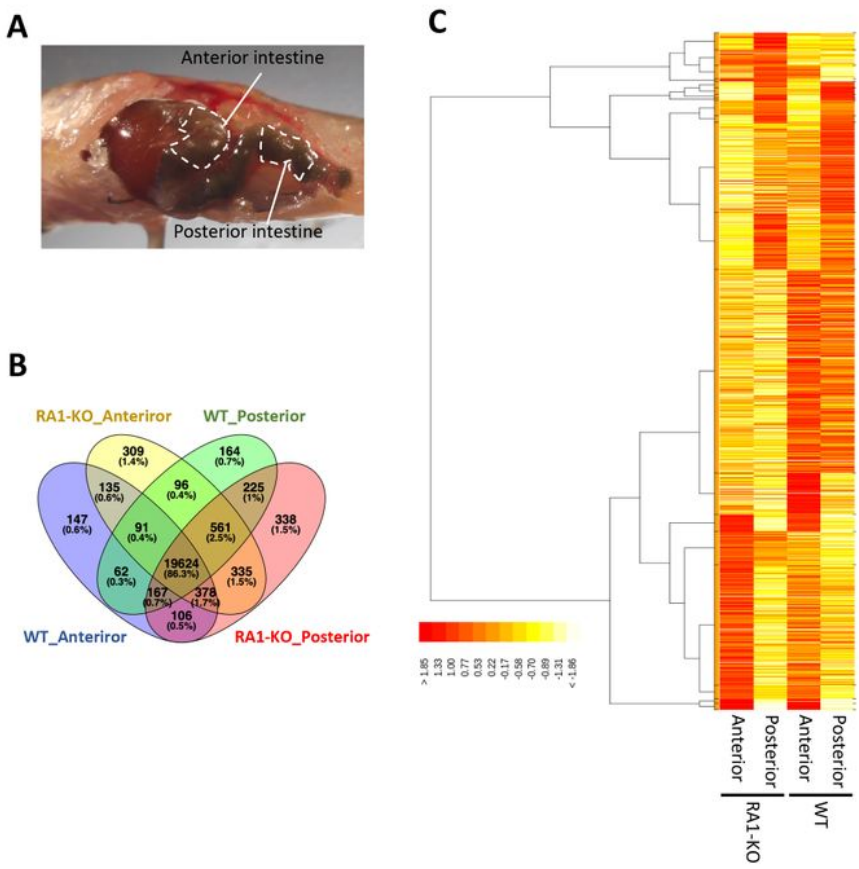

Figure 4

RNA-sequencing (RNA-seq) analysis of samples of the anterior and posterior intestines of WT and IL-17RA1-KO medaka. (A) Complementary DNA libraries were constructed with the selected intestines, as shown in the picture, and the analyzed samples were divided into two sections (anterior and posterior). (B–C) The overall gene-expression patterns are shown for each group (WT_Anterior, RA1-KO_Anterior, WT_Posterior, and RA1-KO Posterior). (B) The Venn diagram shows the numbers of expressed and

overlapping genes expressed in each group. (C) A heat map was also used to visualize differences in the overall gene-expression patterns among the different groups. The heat map was constructed using TCC-GUI software.

Fig. 5.

A

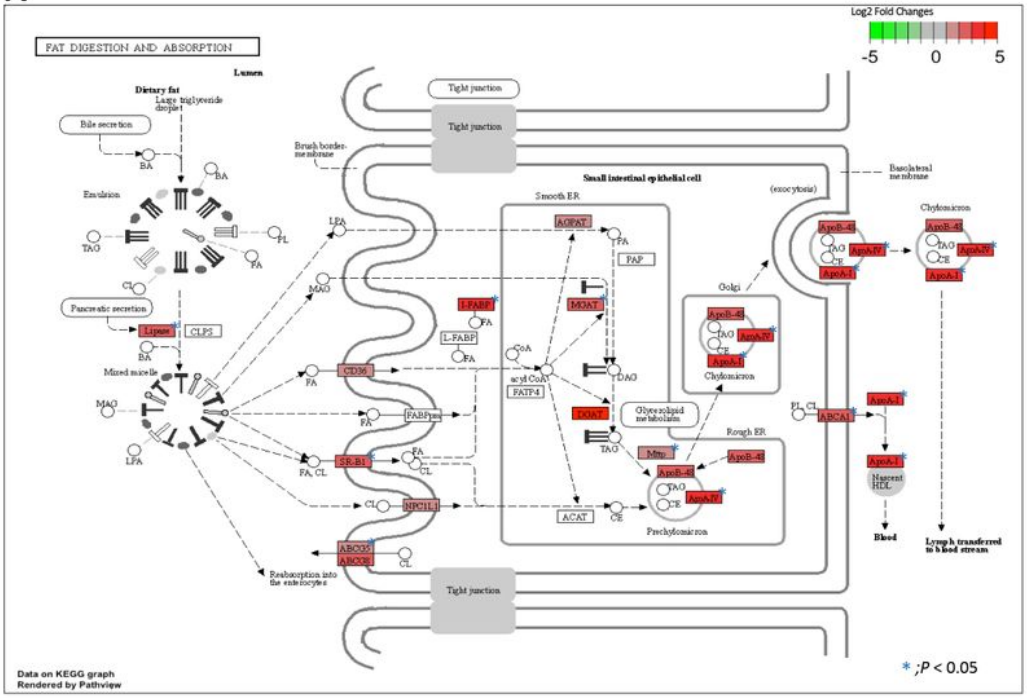

B

GeneID	Gene	Product	FPKM				*p*-value
			Anterior /RA-KO	Posterior /RA-KO	Anterior /WT #1	Posterior /WT #2	#1 vs. #2
ENSORLG00000015744	*apoa1b*	Apolipoprotein A-I	23026.24	4603.74	15041.67	1319.02	0.011
ENSORLG00000009193	*apoa4a*	Apolipoprotein A-IV	6635.77	1034.05	5928.09	542.28	0.012
ENSORLG00000019522	*gucy1b1*	Fatty acid binding protein 2	567.26	242.29	904.99	94.53	0.014
ENSORLG00000027851	*pla2g12b*	Group XIIB secretory phospholipase A2-like protein	62.36	12.51	52.06	7.31	0.021
ENSORLG00000012590	*mogat2*	Monoacylglycerol O-acyltransferase 2	35.09	9.60	31.14	4.56	0.024
ENSORLG00000001304	*scarb1*	Scavenger receptor class B 1	139.15	49.38	113.29	16.60	0.022
ENSORLG00000020504	*abca1*	ATP-binding cassette sub-family A 1	96.58	25.26	53.20	9.68	0.029
ENSORLG00000004629	*abcg8*	ATP binding cassette subfamily G 8	59.89	39.45	58.77	13.57	0.041
ENSORLG00000019412	*mttp*	Microsomal triglyceride transfer protein	92.80	31.67	109.58	29.16	0.050

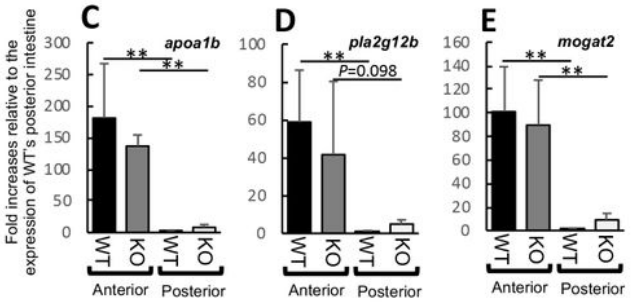

Figure 5

Pathway maps of notable differentially expressed gene (DEG) hits in the anterior intestines, as determined using the Kyoto Encyclopedia of Genes and Genomes (KEGG) database. (A) Medaka anterior

intestines showed enhanced expression of genes related to the “fat digestion and absorption” pathway, as observed in the small intestines of mammals. (B) Nine DEGs were significantly localized to the anterior intestine, and their expression patterns were observed in IL-17RA1-KO medaka. (C–E) Of the nine DEGs, the expression levels of apolipoprotein A-I (apoa1b), group XII B secretory phospholipase A2 (pla2g12b), and monoacylglycerol O-acyltransferase 2 (mogat2) were confirmed by quantitative polymerase chain reaction (qPCR) analysis. **P < 0.01, *P < 0.05 (Student’s t-test or Welch t-test). The data shown were obtained in one experiment with three individual fish (n = 5).

Fig. 5.

A

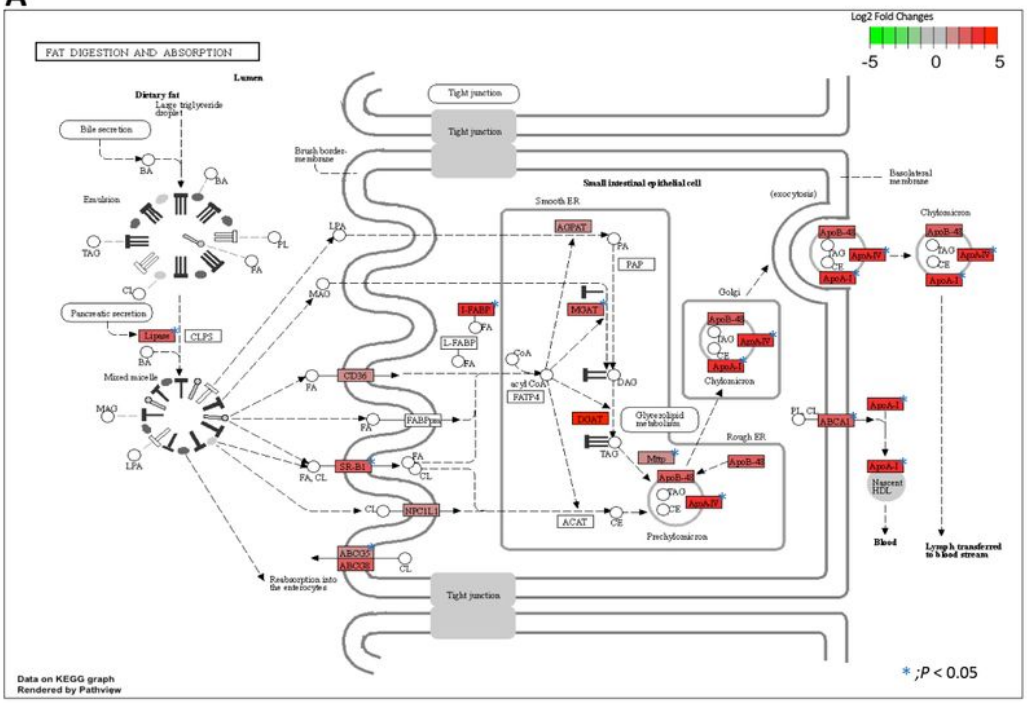

B

GeneID	Gene	Product	FPKM				*p*-value
			Anterior /RA-KO	Posterior /RA-KO	Anterior /WT #1	Posterior /WT #2	#1 vs. #2
ENSORLG00000015744	*apoa1b*	Apolipoprotein A-I	23026.24	4603.74	15041.67	1319.02	0.011
ENSORLG00000009193	*apoa4a*	Apolipoprotein A-IV	6635.77	1034.05	5928.09	542.28	0.012
ENSORLG00000019522	*gucy1b1*	Fatty acid binding protein 2	567.26	242.29	904.99	94.53	0.014
ENSORLG00000027851	*pla2g12b*	Group XIIB secretory phospholipase A2-like protein	62.36	12.51	52.06	7.31	0.021
ENSORLG00000012590	*mogat2*	Monoacylglycerol O-acyltransferase 2	35.09	9.60	31.14	4.56	0.024
ENSORLG00000001304	*scarb1*	Scavenger receptor class B 1	139.15	49.38	113.29	16.60	0.022
ENSORLG00000020504	*abca1*	ATP-binding cassette sub-family A 1	96.58	25.26	53.20	9.68	0.029
ENSORLG00000004629	*abcg8*	ATP binding cassette subfamily G 8	59.89	39.45	58.77	13.57	0.041
ENSORLG00000019412	*mttp*	Microsomal triglyceride transfer protein	92.80	31.67	109.58	29.16	0.050

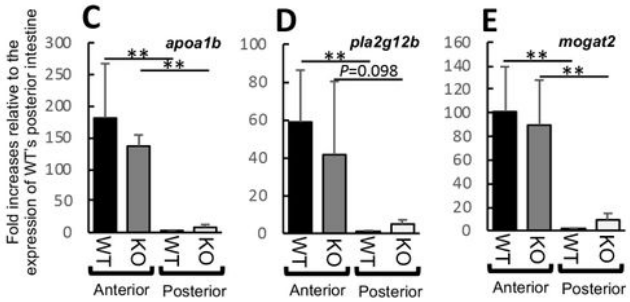

Figure 5

Pathway maps of notable differentially expressed gene (DEG) hits in the anterior intestines, as determined using the Kyoto Encyclopedia of Genes and Genomes (KEGG) database. (A) Medaka anterior intestines showed enhanced expression of genes related to the “fat digestion and absorption” pathway, as observed in the small intestines of mammals. (B) Nine DEGs were significantly localized to the anterior intestine, and their expression patterns were observed in IL-17RA1-KO medaka. (C–E) Of the nine DEGs, the expression levels of apolipoprotein A-I (apoa1b), group XII B secretory phospholipase A2 (pla2g12b), and monoacylglycerol O-acyltransferase 2 (mogat2) were confirmed by quantitative polymerase chain reaction (qPCR) analysis. **P < 0.01, *P < 0.05 (Student’s t-test or Welch t-test). The data shown were obtained in one experiment with three individual fish (n = 5).

Fig. 6.

A

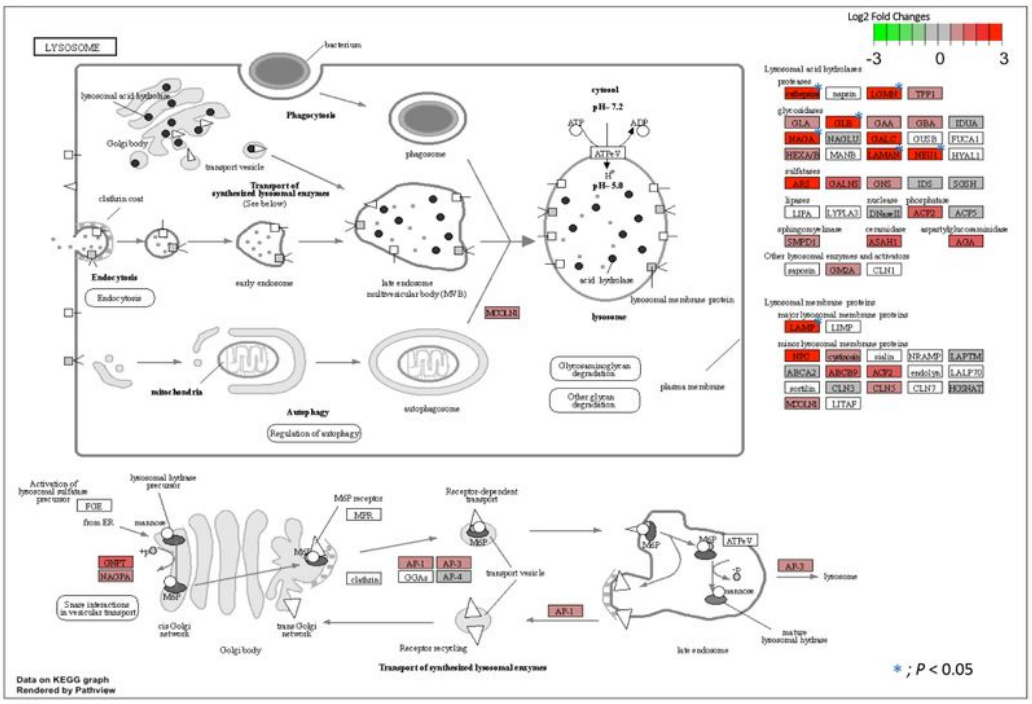

B

GeneID	Gene	Product	FPKM				*p*-value
			Anterior /RA-KO	Posterior /RA-KO	Anterior /WT **#1**	Posterior /WT **#2**	**#1** vs. **#2**
ENSORLG00000017347	*ctsbb*	Cathepsin B	0.23	251.76	0.22	292.91	0.037
ENSORLG00000009533	*lgmn*	Legumain	246.22	3141.40	262.12	5445.87	0.008
ENSORLG00000002057	*neu1*	Neuraminidase 1	9.61	67.11	8.38	129.70	0.012
ENSORLG00000027580	*man2b1*	Mannosidase alpha class 2B 1	10.83	90.93	7.27	82.71	0.018
ENSORLG00000022170	*npc2*	NPC intracellular cholesterol transporter 2	18.36	102.14	14.91	148.89	0.021
ENSORLG00000025883	*ctsz*	Cathepsin Z	122.35	775.66	127.99	1094.52	0.026
ENSORLG00000010823	*ctsc*	Cathepsin C	16.94	113.11	17.37	146.21	0.026
ENSORLG00000009377	*ctsa*	Cathepsin A	37.48	232.48	44.05	296.28	0.036
ENSORLG00000020297	*glb1*	Galactosidase beta 1	4.98	23.59	4.34	26.46	0.042
ENSORLG00000016875	*naga*	Alpha-N-acetylgalactosaminidase	39.33	165.16	31.20	184.91	0.043

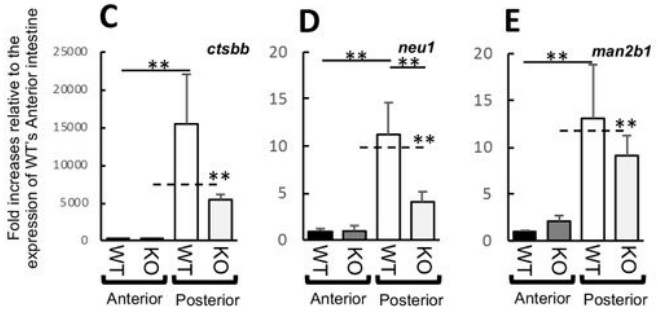

Figure 6

Pathway maps of notable DEGs in the posterior intestines, as determined using the KEGG database. (A) Medaka posterior intestines showed enhanced expression of genes related to the “lysosome” pathway, as participated in lysosome formation. (B) Ten DEGs were significantly localized in the anterior intestines of WT medaka. (C–E) Of these 10 DEGs, the expression levels of cathepsin B (ctsbb), neuraminidase 1 (neu1), and mannosidase alpha class 2B member 1 (man2b1) were confirmed by qPCR analysis. **P <

0.01, *P < 0.05 (Student's t-test or Welch t-test). The data shown were obtained in one experiment with three individual fish (n = 5).

Fig. 6.

A

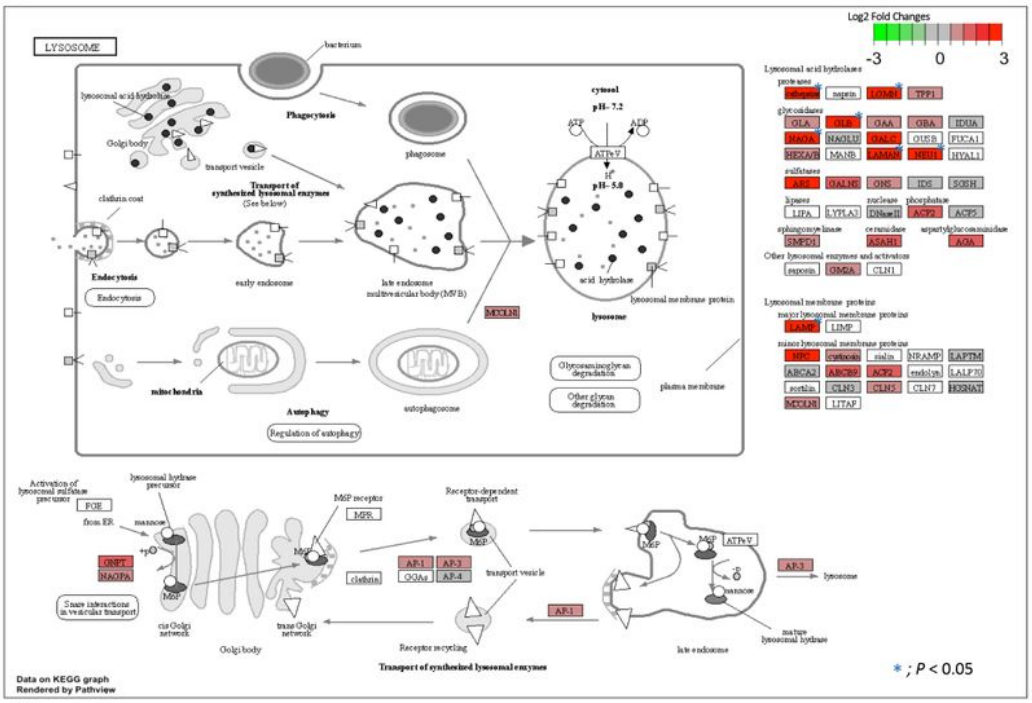

B

GeneID	Gene	Product	FPKM				*p*-value
			Anterior /RA-KO	Posterior /RA-KO	Anterior /WT #1	Posterior /WT #2	#1 vs. #2
ENSORLG00000017347	*ctsbb*	Cathepsin B	0.23	251.76	0.22	292.91	0.037
ENSORLG00000009533	*lgmn*	Legumain	246.22	3141.40	262.12	5445.87	0.008
ENSORLG00000002057	*neu1*	Neuraminidase 1	9.61	67.11	8.38	129.70	0.012
ENSORLG00000027580	*man2b1*	Mannosidase alpha class 2B 1	10.83	90.93	7.27	82.71	0.018
ENSORLG00000022170	*npc2*	NPC intracellular cholesterol transporter 2	18.36	102.14	14.91	148.89	0.021
ENSORLG00000025883	*ctsz*	Cathepsin Z	122.35	775.66	127.99	1094.52	0.026
ENSORLG00000010823	*ctsc*	Cathepsin C	16.94	113.11	17.37	146.21	0.026
ENSORLG00000009377	*ctsa*	Cathepsin A	37.48	232.48	44.05	296.28	0.036
ENSORLG00000020297	*glb1*	Galactosidase beta 1	4.98	23.59	4.34	26.46	0.042
ENSORLG00000016875	*naga*	Alpha-N-acetylgalactosaminidase	39.33	165.16	31.20	184.91	0.043

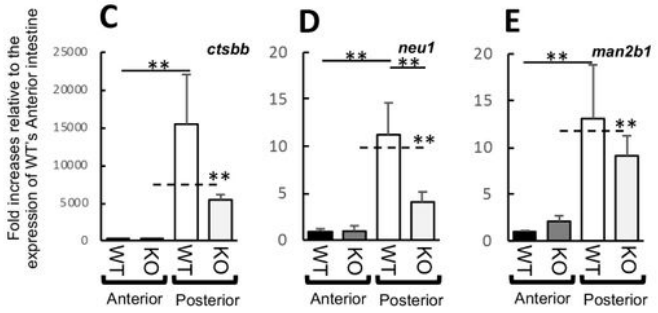

Figure 6

Pathway maps of notable DEGs in the posterior intestines, as determined using the KEGG database. (A) Medaka posterior intestines showed enhanced expression of genes related to the "lysosome" pathway, as participated in lysosome formation. (B) Ten DEGs were significantly localized in the anterior intestines of

WT medaka. (C–E) Of these 10 DEGs, the expression levels of cathepsin B (ctsbb), neuraminidase 1 (neu1), and mannosidase alpha class 2B member 1 (man2b1) were confirmed by qPCR analysis. **P < 0.01, *P < 0.05 (Student's t-test or Welch t-test). The data shown were obtained in one experiment with three individual fish (n = 5).

Fig. 7.

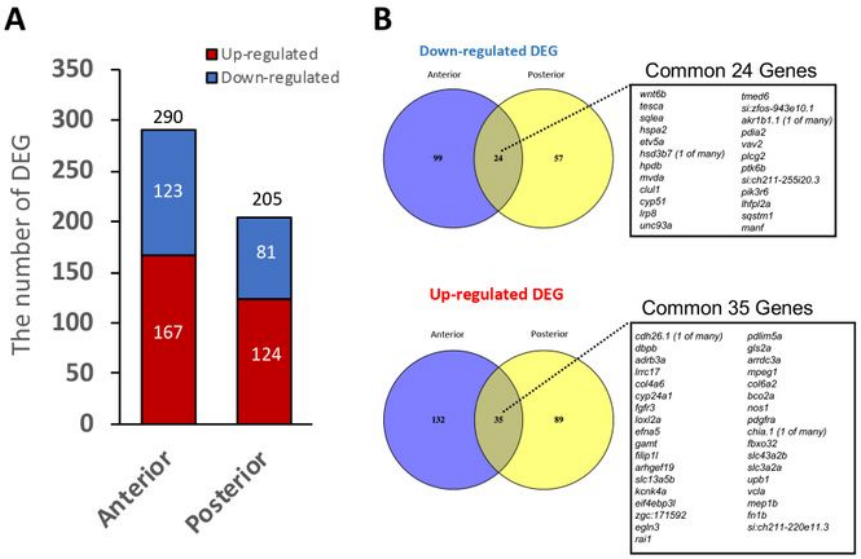

Figure 7

The numbers of DEGs detected in the anterior and posterior intestines of IL-17RA1-KO medaka compared to that of WT. (A) In the anterior intestine, 290 DEGs were identified between WT and IL-17RA1-KO. In addition, 205 DEGs were identified in the posterior intestine. (B) Of these DEGs, 24 genes were consistently down-regulated in both the anterior and posterior intestines of IL-17RA1-KO medaka. In addition, 35 DEGs were consistently up-regulated in both the anterior and posterior intestines of IL-17RA1-KO medaka.

Fig. 7.

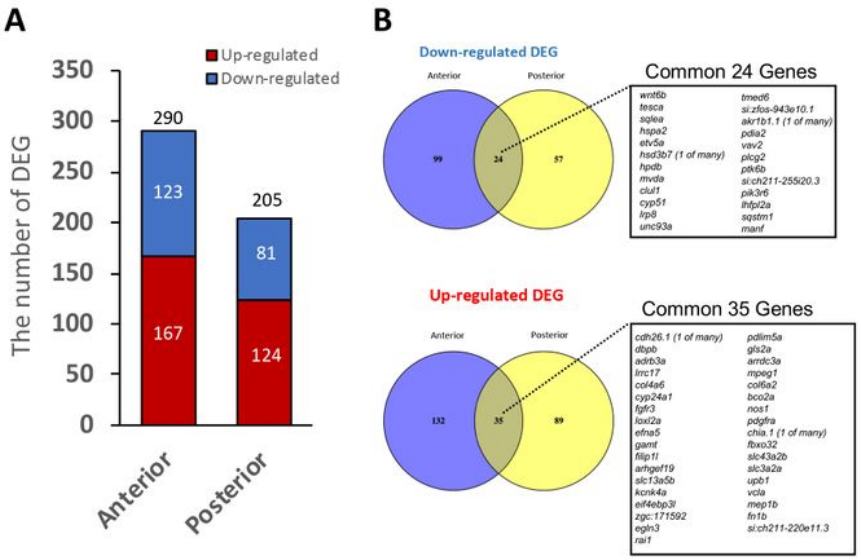

Figure 7

The numbers of DEGs detected in the anterior and posterior intestines of IL-17RA1-KO medaka compared to that of WT. (A) In the anterior intestine, 290 DEGs were identified between WT and IL-17RA1-KO. In addition, 205 DEGs were identified in the posterior intestine. (B) Of these DEGs, 24 genes were consistently down-regulated in both the anterior and posterior intestines of IL-17RA1-KO medaka. In addition, 35 DEGs were consistently up-regulated in both the anterior and posterior intestines of IL-17RA1-KO medaka.

Fig. 8.

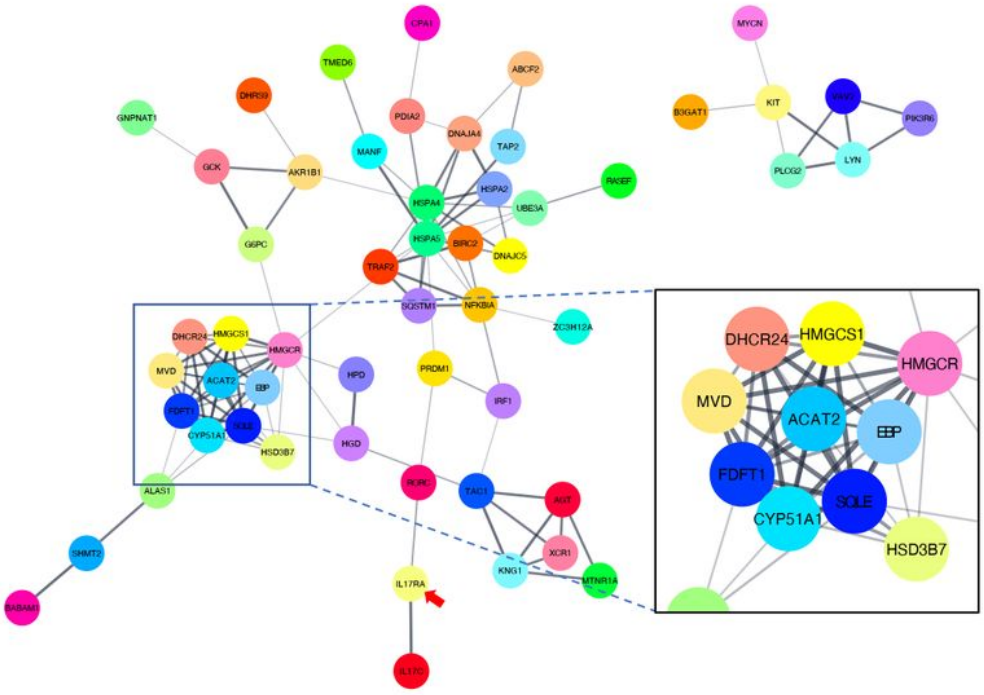

Figure 8

Predicted interactions between DEGs down-regulated in IL-17RA1-KO and IL-17RA medaka. The interaction network between these genes was defined using the String App database (Cytoscape). Of 123 DEGs identified, 47 formed the most complex cluster and contained IL-17RA. The gene cluster contained the ligands of IL-17RA, il17c, and the master transcriptional factor of IL-17-producing lymphocytes, rorc. Additionally, an aggregation of genes, including the mevalonate pathway-related genes, mvda, acat2, hmgcs1, and hmgcr, formed in the cluster of 47 DEGs. The red arrow points to IL-17RA.

Fig. 8.

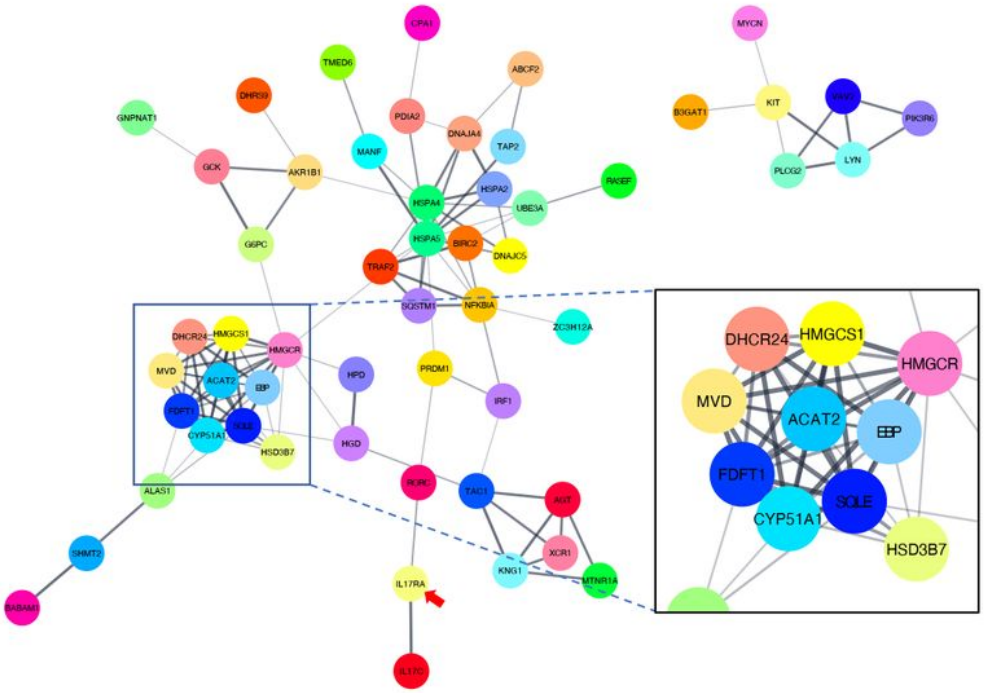

Figure 8

Predicted interactions between DEGs down-regulated in IL-17RA1-KO and IL-17RA medaka. The interaction network between these genes was defined using the String App database (Cytoscape). Of 123 DEGs identified, 47 formed the most complex cluster and contained IL-17RA. The gene cluster contained the ligands of IL-17RA, il17c, and the master transcriptional factor of IL-17-producing lymphocytes, rorc. Additionally, an aggregation of genes, including the mevalonate pathway-related genes, mvda, acat2, hmgcs1, and hmgcr, formed in the cluster of 47 DEGs. The red arrow points to IL-17RA.

Fig. 9.

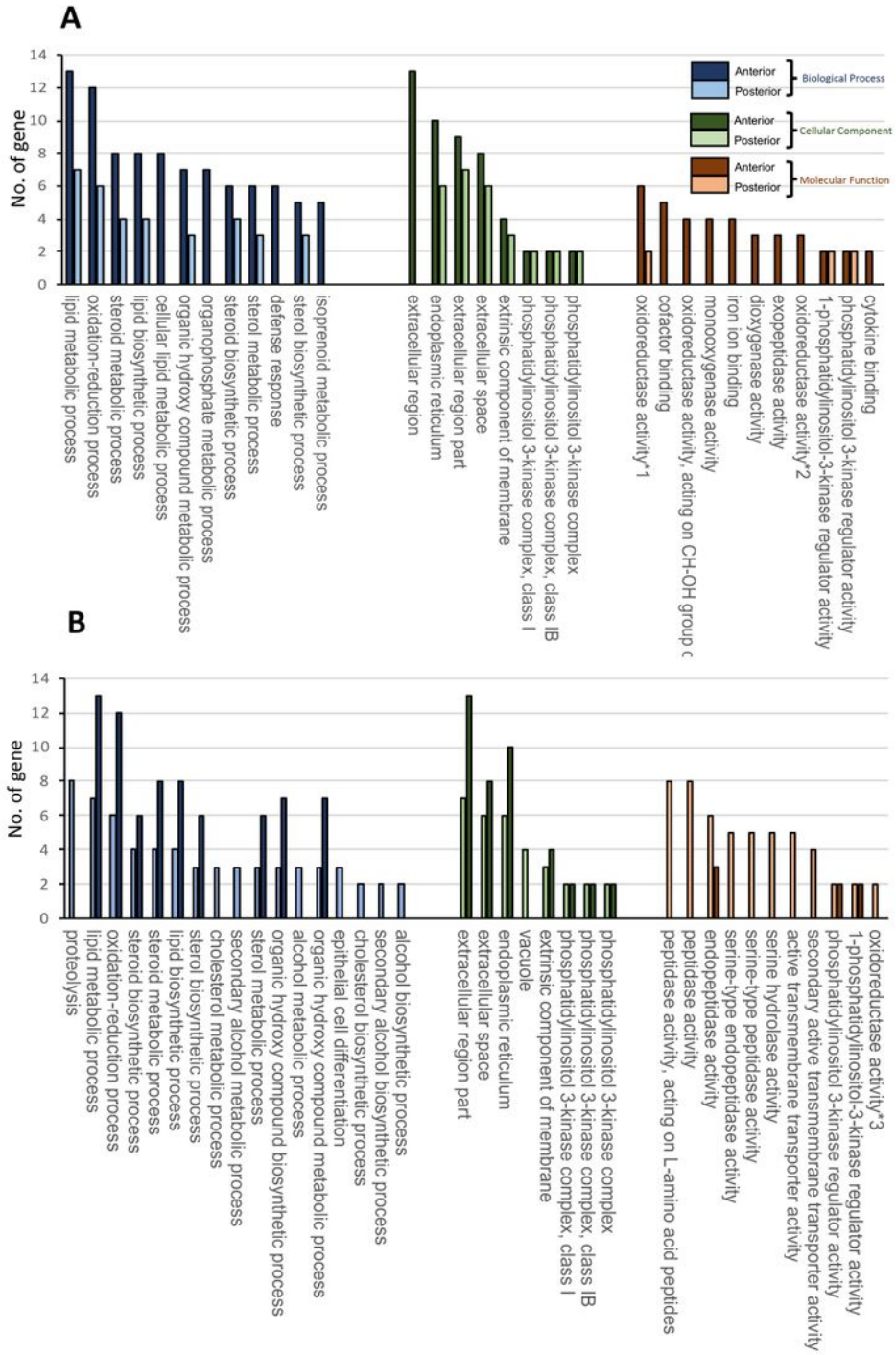

Figure 9

Top 12 classification of Gene Ontology (GO) enrichment of down-regulated DEGs in the anterior and posterior intestines of IL-17RA1-KO. (A) Down-regulated DEGs in the anterior intestine of IL-17RA1-KO medaka were related to GO terms describing various metabolic processes including lipid metabolism, steroid metabolism and lipid biosynthesis and oxidation reduction, within the category of biological processes (BPs). Immune terms such as defense response (BP category) and cytokine binding (molecular function category) were included among the top 12 terms with the most hits. (B) Among down-regulated DEGs in the posterior intestine of IL-17RA1-KO medaka, proteolysis was the BP term with the most hits; lipid metabolism-related and oxidation-reduction terms were also identified as hits, as observed in the anterior intestine. The numbers with asterisks indicate cases where the full-length official GO terms were abbreviated. The complete names of the official GO terms are as follows: *1: oxidoreductase activity, acting on paired donors, with incorporation or reduction of molecular oxygen, *2: oxidoreductase activity, acting on the CH-OH group of donors, NAD or NADP as acceptor, *3: oxidoreductase activity, acting on paired donors, with incorporation or reduction of molecular oxygen, NAD(P)H as one donor, and incorporation of one atom of oxygen.

Fig. 9.

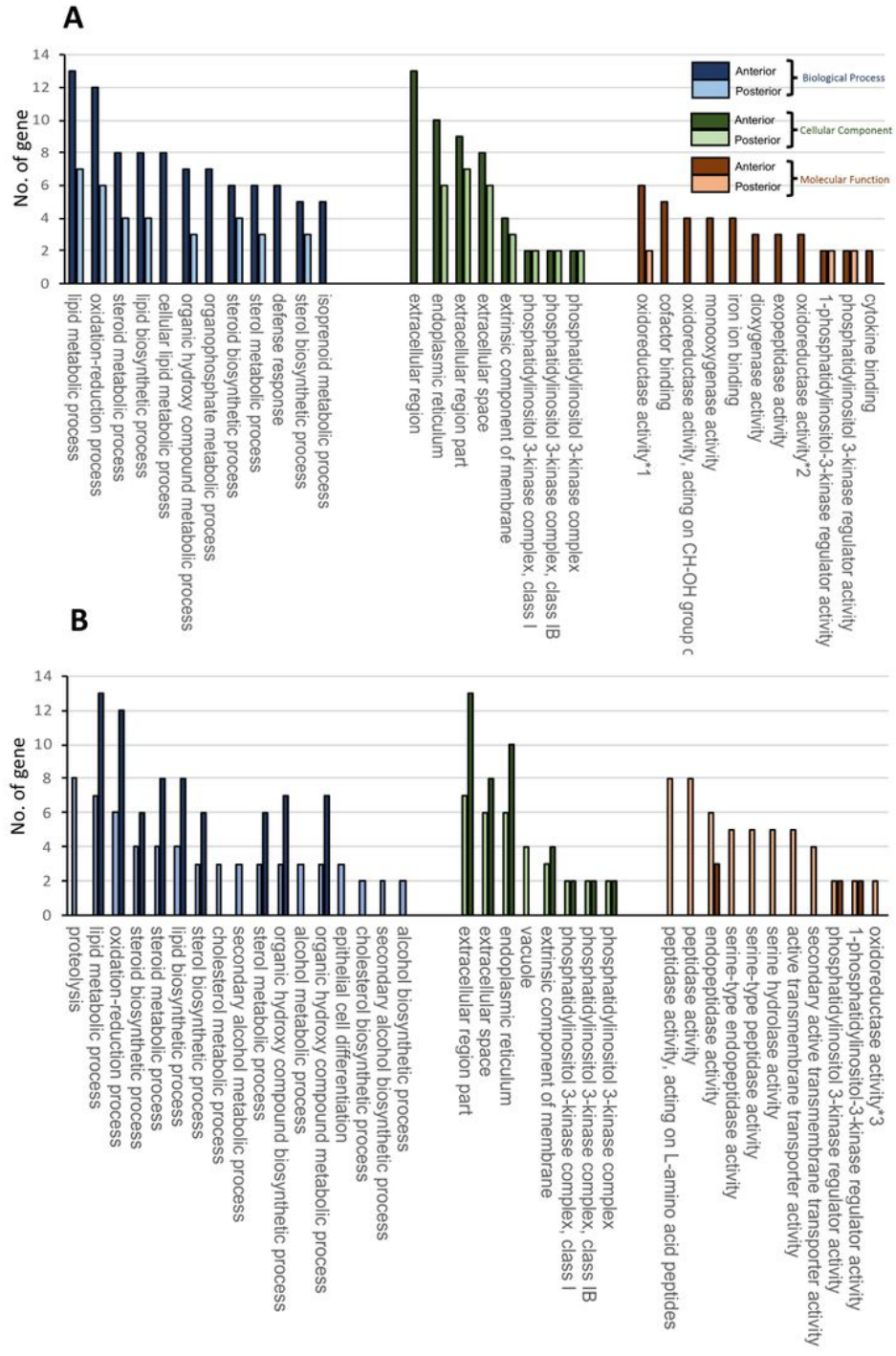

Figure 9

Top 12 classification of Gene Ontology (GO) enrichment of down-regulated DEGs in the anterior and posterior intestines of IL-17RA1-KO. (A) Down-regulated DEGs in the anterior intestine of IL-17RA1-KO medaka were related to GO terms describing various metabolic processes including lipid metabolism, steroid metabolism and lipid biosynthesis and oxidation reduction, within the category of biological processes (BPs). Immune terms such as defense response (BP category) and cytokine binding (molecular

function category) were included among the top 12 terms with the most hits. (B) Among down-regulated DEGs in the posterior intestine of IL-17RA1-KO medaka, proteolysis was the BP term with the most hits; lipid metabolism-related and oxidation-reduction terms were also identified as hits, as observed in the anterior intestine. The numbers with asterisks indicate cases where the full-length official GO terms were abbreviated. The complete names of the official GO terms are as follows: *1: oxidoreductase activity, acting on paired donors, with incorporation or reduction of molecular oxygen, *2: oxidoreductase activity, acting on the CH-OH group of donors, NAD or NADP as acceptor, *3: oxidoreductase activity, acting on paired donors, with incorporation or reduction of molecular oxygen, NAD(P)H as one donor, and incorporation of one atom of oxygen.

Fig. 10.

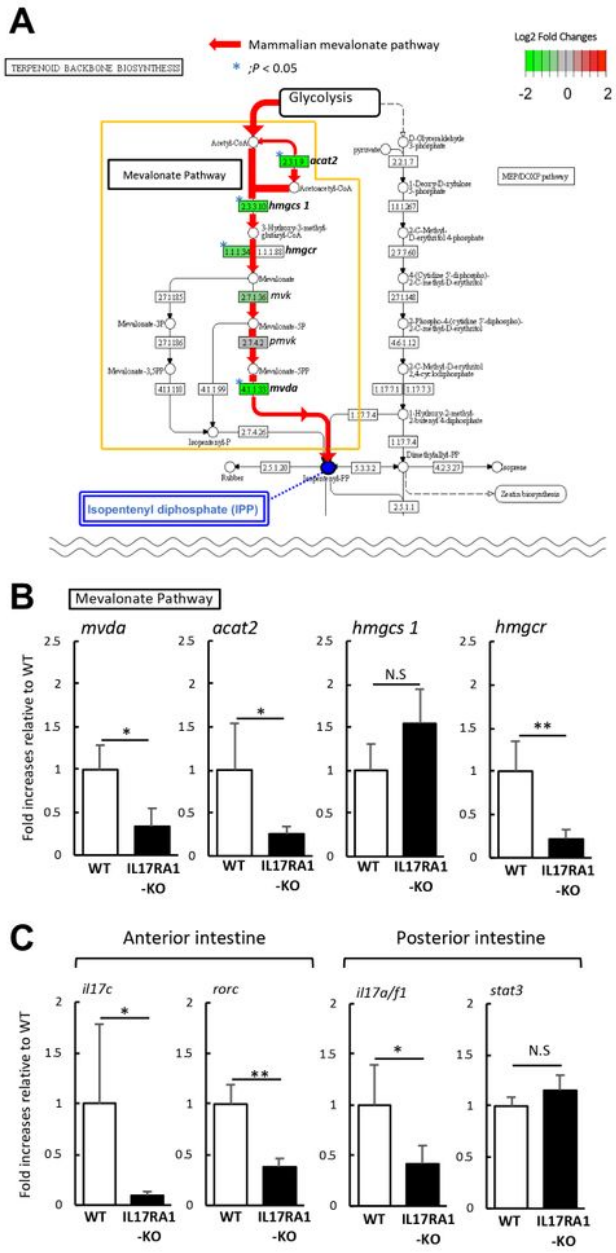

Figure 10

The reduction of the mevalonate pathway-related genes in IL-17RA1-KO medaka intestines. (A, B) In the anterior intestine of IL-17RA1-KO medaka; four of six enzyme-encoding genes participating in the mevalonate pathway were significantly down-regulated as shown by RNA-seq analyses (A). Of these four genes, the reduction of acat2 and hmgcs1 was confirmed by real-time qPCR. (C) qPCR analysis was also used to confirm the reduced expression of IL-17 signaling-related genes, il17c and rorc, observed by RNA-

seq. **P < 0.01, *P < 0.05 (Student's t-test or Welch t-test). The data shown were obtained in one experiment with three individual fish (n = 5).

Fig. 10.

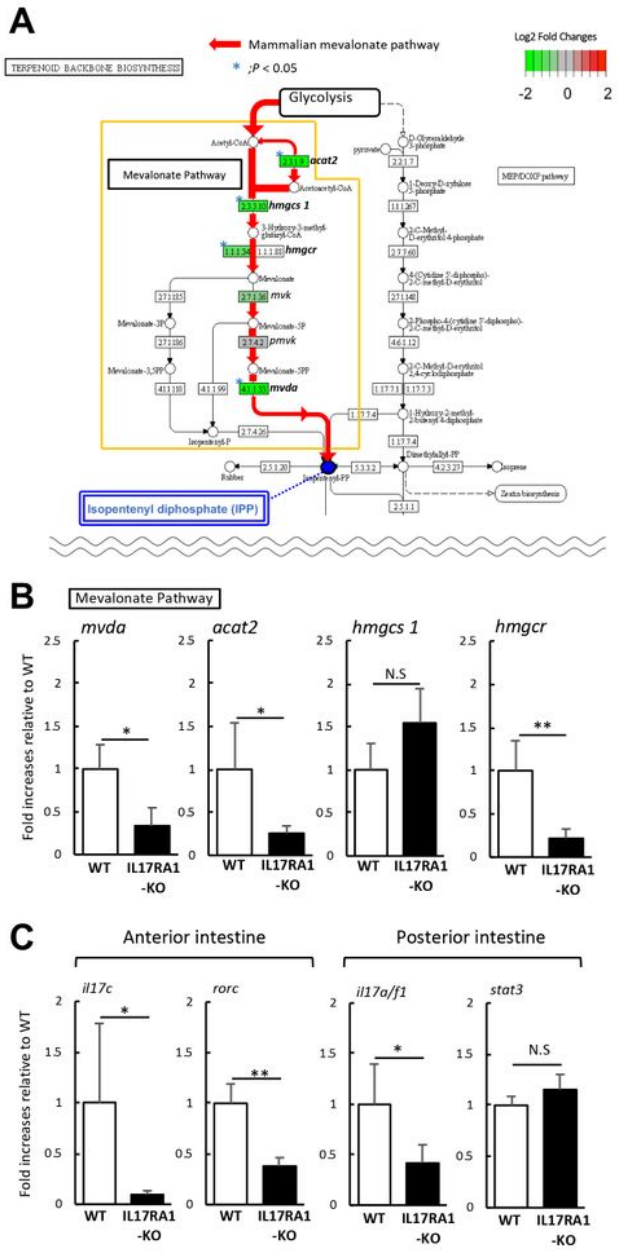

Figure 10

The reduction of the mevalonate pathway-related genes in IL-17RA1-KO medaka intestines. (A, B) In the anterior intestine of IL-17RA1-KO medaka; four of six enzyme-encoding genes participating in the mevalonate pathway were significantly down-regulated as shown by RNA-seq analyses (A). Of these four

genes, the reduction of acat2 and hmgcs1 was confirmed by real-time qPCR. (C) qPCR analysis was also used to confirm the reduced expression of IL-17 signaling-related genes, il17c and rorc, observed by RNA-seq. **P < 0.01, *P < 0.05 (Student's t-test or Welch t-test). The data shown were obtained in one experiment with three individual fish (n = 5).

Supplementary Files

This is a list of supplementary files associated with this preprint. Click to download.

- Table1..xlsx
- Table1..xlsx
- Suppl.materialsSRYO.pdf
- Suppl.materialsSRYO.pdf
- Table2..xlsx
- Table2..xlsx
- Suppl.tablesS1S7.xlsx
- Suppl.tablesS1S7.xlsx
- Suppl.FigsSRYO2.pdf
- Suppl.FigsSRYO2.pdf
- Suppl.FigsSRYO3.pdf
- Suppl.FigsSRYO3.pdf
- Suppl.FigsSRYO3.pdf
- Suppl.FigsSRYO3.pdf
- Suppl.tablesS1S7.xlsx
- Suppl.tablesS1S7.xlsx